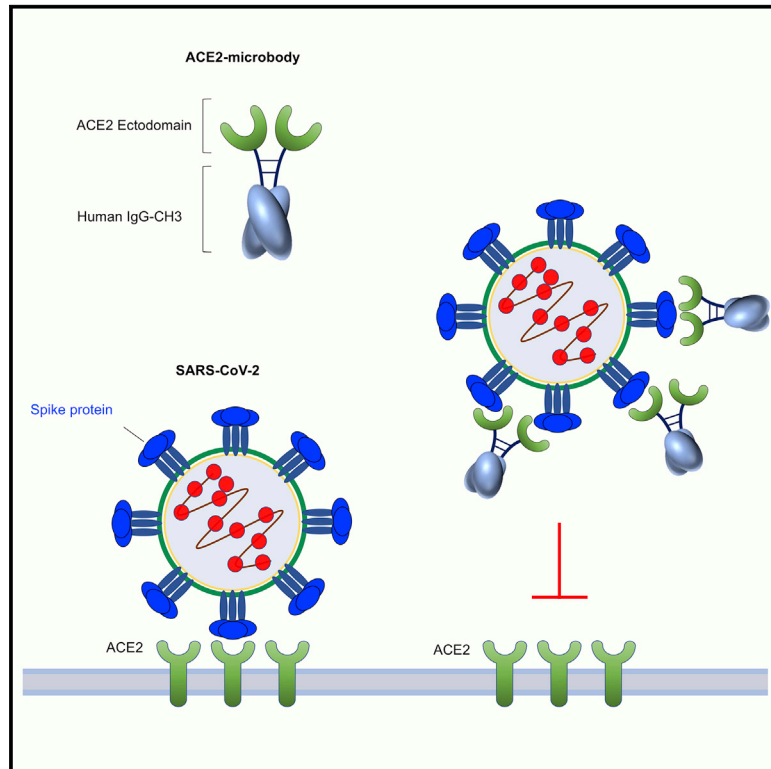**Article**

An ACE2 Microbody Containing a Single Immunoglobulin Fc Domain Is a Potent Inhibitor of SARS-CoV-2

Graphical Abstract

Authors

Takuya Tada, Chen Fan,
Jennifer S. Chen, ..., Craig B. Wilen,
Crina M. Nimigean, Nathaniel R. Landau

Correspondence

nathaniel.landau@med.nyu.edu

In Brief

Tada et al. generate an ACE2 "microbody" in which the ACE2 ectodomain is fused to immunoglobulin heavy chain Fc domain 3. The ACE2 microbody protein potently inhibits the entry of SARS-CoV-2 spike protein pseudotyped virus into cells and replication of live SARS-CoV-2 *in vitro* and in a mouse model.

Highlights

- An ACE2 microbody inhibits entry of SARS-CoV-2 spike protein pseudotyped virus

- ACE2 microbody inhibits replication of live virus *in vitro* and in a mouse model

- Antiviral potency of the ACE2 microbody is 10-fold higher than that of soluble ACE2

- ACE2 microbody inhibits entry of the D614G spike and other β coronavirus spikes

CellPress

Article

An ACE2 Microbody Containing a Single Immunoglobulin Fc Domain Is a Potent Inhibitor of SARS-CoV-2

Takuya Tada,[1] Chen Fan,[2] Jennifer S. Chen,[3,4] Ramanjit Kaur,[1] Kenneth A. Stapleford,[1] Harry Gristick,[5] Belinda M. Dcosta,[1] Craig B. Wilen,[3,4] Crina M. Nimigean,[2] and Nathaniel R. Landau[1,6,*]

[1]Department of Microbiology, NYU Langone Medical Center, New York, NY 10016, USA
[2]Department of Anesthesiology, Weill Cornell Medical College, New York, NY 10065, USA
[3]Department of Laboratory Medicine, Yale School of Medicine, New Haven, CT 06520, USA
[4]Department of Immunobiology, Yale School of Medicine, New Haven, CT 06520, USA
[5]Division of Biology and Biological Engineering, California Institute of Technology, Pasadena, CA 91125, USA
[6]Lead Contact
*Correspondence: nathaniel.landau@med.nyu.edu
https://doi.org/10.1016/j.celrep.2020.108528

SUMMARY

Soluble forms of angiotensin-converting enzyme 2 (ACE2) have recently been shown to inhibit severe acute respiratory syndrome coronavirus 2 (SARS-CoV-2) infection. We report on an improved soluble ACE2, termed a "microbody," in which the ACE2 ectodomain is fused to Fc domain 3 of the immunoglobulin (Ig) heavy chain. The protein is smaller than previously described ACE2-Ig Fc fusion proteins and contains an H345A mutation in the ACE2 catalytic active site that inactivates the enzyme without reducing its affinity for the SARS-CoV-2 spike. The disulfide-bonded ACE2 microbody protein inhibits entry of SARS-CoV-2 spike protein pseudotyped virus and replication of live SARS-CoV-2 in vitro and in a mouse model. Its potency is 10-fold higher than soluble ACE2, and it can act after virus bound to the cell. The microbody inhibits the entry of β coronaviruses and virus with the variant D614G spike. The ACE2 microbody may be a valuable therapeutic for coronavirus disease 2019 (COVID-19) that is active against viral variants and future coronaviruses.

INTRODUCTION

As the severe acute respiratory syndrome coronavirus 2 (SARS-CoV-2) continues to spread worldwide, there is an urgent need for preventative vaccine and improved therapeutics for treatment of COVID-19. The development of therapeutic agents that block specific steps of the coronavirus replication cycle will be highly valuable both for treatment and prophylaxis. Coronavirus replication consists of attachment, uncoating, replication, translation, assembly, and release, all of which are potential drug targets. Virus entry is particularly advantageous because as the first step in virus replication, it spares target cells from becoming infected and because drugs that block entry do not need to be cell permeable as the targets are externally exposed. In SARS-CoV-2 entry, the virus attaches to the target cell through the interaction of the spike glycoprotein with its receptor, the angiotensin-converting enzyme 2 (ACE2) (Li, 2015; Li et al., 2003, 2005), a plasma membrane protein carboxypeptidase that degrades angiotensin II to angiotensin-(1–7) (Ang-(1–7)), a vasodilator that promotes sodium transport in the regulation of cardiac function and blood pressure (Kuba et al., 2010; Riordan, 2003; Tikellis and Thomas, 2012). ACE2 binding triggers spike protein-mediated fusion of the viral envelope with the cell plasma membrane or intracellular endosomal membranes. The spike protein is synthesized as a single poly-peptide that is cleaved by the cellular protease furin into S1 and S2 subunits in the endoplasmic reticulum and then further processed by TMPRSS2 on target cells (Glowacka et al., 2011; Hoffmann et al., 2020; Matsuyama et al., 2010; Shulla et al., 2011). The S1 subunit contains the receptor binding domain (RBD), which binds to ACE2, while S2 mediates virus-cell fusion (Belouzard et al., 2012; Fehr and Perlman, 2015; Heald-Sargent and Gallagher, 2012; Li et al., 2006; Shang et al., 2020). Cells that express ACE2 are potential targets of the virus. These include cells in the lungs, arteries, heart, kidney, and intestines (Harmer et al., 2002; Ksiazek et al., 2003; Leung et al., 2003).

The use of soluble receptors to prevent virus entry by competitively binding to viral envelope glycoproteins was first explored for HIV-1 with soluble CD4. In early studies, a soluble form of CD4 deleted for the transmembrane and cytoplasmic domains was found to block virus entry in vitro (Daar et al., 1990; Haim et al., 2009; Orloff et al., 1993; Schenten et al., 1999; Sullivan et al., 1998). Fusion of the protein to an immunoglobulin Fc region, termed an "immunoadhesin," increased the avidity for gp120 by dimerizing the protein and served to increase the half-life of the protein in vivo. An enhanced soluble CD4-Ig containing a peptide derived from the HIV-1 coreceptor CCR5 was found to potently block infection and to protect rhesus macaques from infection (Chiang et al., 2012). The soluble receptor approach to blocking
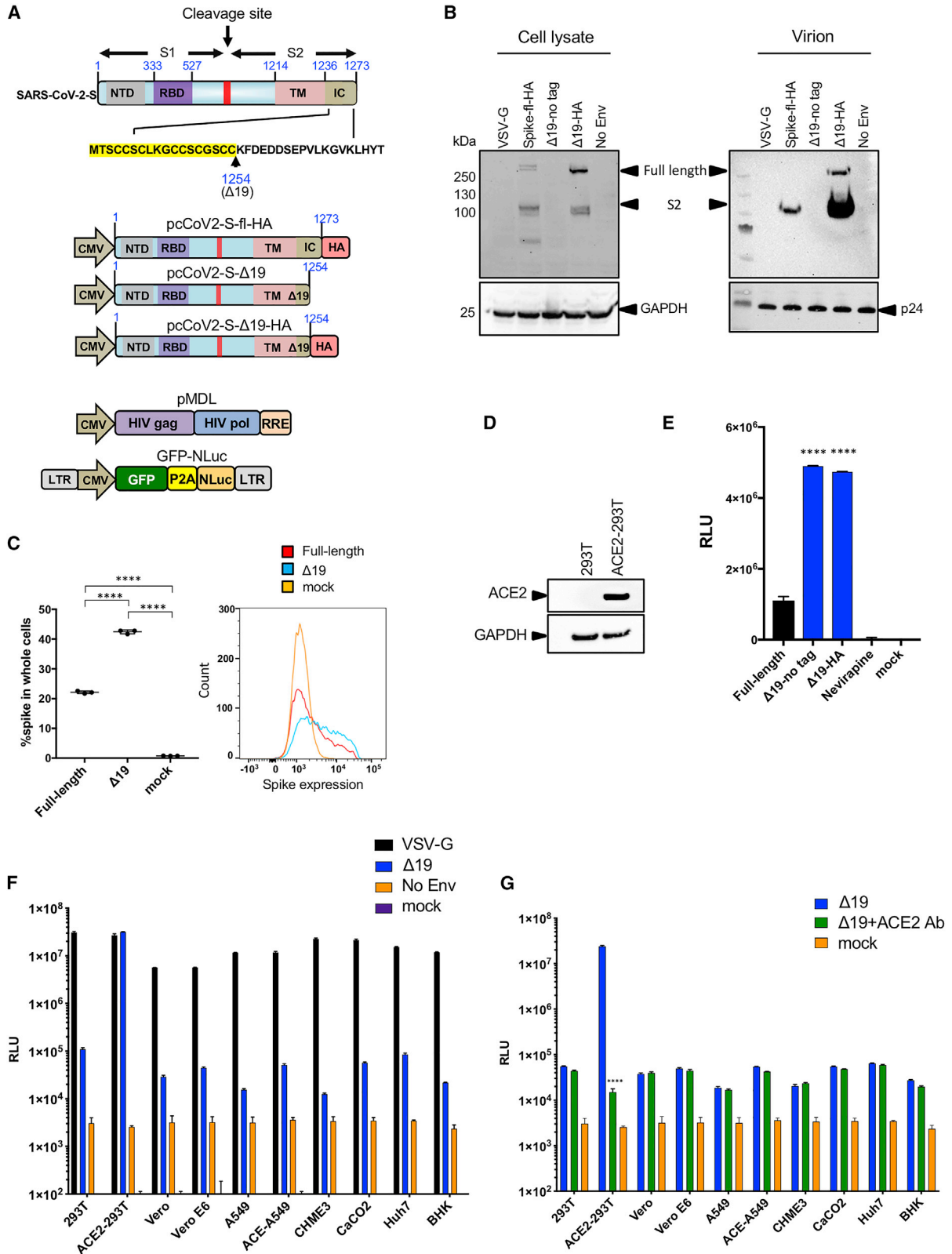
(legend on next page)

virus entry has been recently applied to SARS-CoV-2 through the use of recombinant human soluble ACE2 protein (hrsACE2) (Kuba et al., 2005; Monteil et al., 2020; Wysocki et al., 2010) or hrsACE2-immunoglobulin G (IgG), which encodes soluble ACE2 and the Fc region of the human IgG (Case et al., 2020; Lei et al., 2020; Qian and Hu, 2020), which were shown to inhibit SARS-CoV and SARS-CoV-2 entry in a mouse model. In phase 1 and 2 clinical trials (Haschke et al., 2013; Khan et al., 2017), the protein showed partial antiviral activity but short half-life. Addition of the Fc region increased the half-life of the protein *in vivo*. A potential concern with the addition of the Ig Fc region is the possibility of enhancement, similar to what occurs with antibody-dependent enhancement in which anti-spike protein antibody attaches to Fc receptors on immune cells, facilitating infection rather than preventing it (Eroshenko et al., 2020).

We report here on a soluble human ACE2 "microbody" in which the ACE2 ectodomain is fused to domain 3 of the IgG heavy chain Fc region (IgG-CH3) (Maute et al., 2015). The IgG-CH3 Fc domain served to dimerize the protein, increasing its affinity for the SARS-CoV-2 S, and decreased the molecular mass of the protein as compared with fusion with full-length Fc. The ACE2 microbody did not bind to cell surface Fc receptor, reducing any possibility of infection enhancement. Mutation of the active site H345 to alanine in the ACE2 microbody protein, a mutation that has been shown to inactivate ACE2 catalytic activity (Guy et al., 2005), did not decrease its affinity for the spike protein. The dimeric ACE2 microbody had about 10-fold higher antiviral activity than soluble ACE2, which was also a dimer, and had a higher affinity for virion binding. The ACE2 microbody blocked virus entry into ACE2.293T cells that overexpressed ACE2, as well as all of the cell lines tested. It was active against the D614G variant spike protein and against a panel of β coronavirus spike proteins and protected human ACE2 transgenic mice against infection.

RESULTS

SARS-CoV-2 Δ19 Spike Protein Was Incorporated in Pseudotyped Virion and Had Higher Infectivity

As a means to study SARS-CoV-2 entry, we developed an assay based on SARS-CoV-2 spike protein pseudotyped lentiviral re-porter viruses. The viruses package a lentiviral vector genome that encodes nanoluciferase and GFP separated by a P2A self-processing peptide, providing a convenient means to titer the virus and the ability to use two different assays to measure infection. To pseudotype the virions, we constructed expression vectors for the full-length SARS-CoV-2 S and for a Δ19 variant, deleted for the carboxy-terminal 19 amino acids that remove a reported endoplasmic reticulum retention sequence that blocks transit of the spike protein to the cell surface (Giroglou et al., 2004) (Figure 1A). The vectors were constructed with or without a carboxy-terminal hemagglutinin (HA) epitope tag. Pseudotyped viruses were produced in 293T cells cotransfected with the dual nanoluciferase/GFP reporter lentiviral vector pLen-ti.GFP.NLuc, Gag/Pol expression vector pMDL and full-length spike protein, Δ19 spike protein, vesicular stomatitis virus G protein (VSV-G) expression vector, or without an envelope glycoprotein expression vector. Immunoblot analysis showed that full-length and Δ19 spike proteins were expressed and processed into the cleaved S2 protein (S1 is not visible because it lacks an epitope tag). Analysis of the virions showed that the Δ19 spike protein was packaged into virions at >20-fold higher levels than the full-length protein (Figure 1B). This difference was not the result of differences in virion production because similar amounts of virion p24 capsid protein were present in the cell supernatant. Analysis of the transfected 293T cells by flow cytometry showed a minor increase in the amount of cell surface Δ19 spike protein as compared with full length (Figure 1C), suggesting that deletion of the endoplasmic reticulum retention signal was not the primary cause of the increased virion packaging of the Δ19 spike protein and may result from an inhibitory effect of the spike protein cytoplasmic tail on virion incorporation. As a suitable target cell line, we established a clonal, stably transfected 293T cell line that expressed high levels of ACE2 (Figures 1D and S1). A comparison of the infectivity of the viruses on ACE2.293T cells showed that the Δ19 spike protein pseudotype was about 2.5-fold more infectious than the full-length spike protein pseudotype (Figure 1E). The HA-tag had no effect on infectivity, and the nevirapine control demonstrated that the luciferase activity was the result of bona fide infection and not carried-over luciferase in the virus-containing supernatant.

Figure 1. Δ19 SARS-CoV-2 Pseudotyped Lentiviral Virion Infection of ACE2.293T Cells and ACE2 Expressing Cell Lines

(A) The domain structure of the SARS-CoV-2 spike protein is diagrammed above. Yellow shading indicates the amino acids of the cytoplasmic domain retained following truncation of the 19 carboxy-terminal amino acids (Δ19). Vectors encoding full-length (fl) codon-optimized SARS-CoV-2 spike protein or truncated Δ19 spike protein, with or without a carboxy-terminal HA-tag and the dual nanoluciferase/GFP lentiviral vector pLenti.NLuc.GFP used to generate pseudotyped lentiviral particles, are diagrammed (below).

(B) SARS-CoV-2 spike proteins on pseudotyped lentiviral virions were analyzed. Transfected producer cell lysates (left) and supernatant virions (right) were analyzed on an immunoblot probed with anti-HA antibody. Cell lysate blots were probed with anti-GAPDH to normalize protein loading, and virion blots were probed for HIV-1 p24 to normalize for virions.

(C) 293T cells transfected with SARS-CoV-2 spike protein expression vectors were analyzed by flow cytometry to detect the protein at the plasma membrane.

(D) HA-tagged ACE2 expressed in control transfected 293T and clonal ACE2.293T cells were analyzed on an immunoblot probed with anti-HA antibody.

(E) ACE2.293T cells were infected with virus pseudotyped by full-length or SARS-CoV-2 Δ19 spike proteins. Two days post-infection, infectivity was measured by luciferase assay. The reverse transcriptase inhibitor nevirapine was added to one sample to control for free luciferase enzyme contamination of the virus stock.

(F) A panel of cell lines were infected with VSV-G, SARS-CoV-2 Δ19 spike protein, or no envelope (no Env) pseudotyped lentivirus (MOI = 0.2). Luciferase activity was measured 2 days post-infection.

(G) ACE2.293T cells were treated with ACE2 antibody (1:20) for 30 min at room temperature, and SARS-CoV-2 Δ19 virus was added on the cells. After 2 days of incubation, luciferase activity was measured. The data are represented as the mean of triplicates ± standard deviation. Statistical significance was calculated with the Student's t test. The experiment was done twice with similar results.

IC, intracellular domain; LTR, long terminal repeat; NTD, N-terminal domain; RBD, receptor binding domain; RRE, Rev response element; TM, transmembrane domain.

To determine the cell-type tropism of the pseudotyped virus, we tested several standard laboratory cell lines for susceptibility to infection to the Δ19 spike protein pseudotyped virus. The VSV-G pseudotype, which has very high infectivity on most cell types, was tested for comparison, and virus lacking a glycoprotein was included to control for potential receptor-independent virus uptake. The results showed high infectivity of the Δ19 spike protein pseudotyped virus on ACE2.293T cells, intermediate infectivity on 293T, Vero, Vero E6, A549, ACE2.A549, CaCO$_2$, and Huh7, and low infectivity on A549, CHME3, and BHK (Figure 1F). Vero and Vero E6 are African Green Monkey cells and as such express TRIM5α, which likely accounts for the slight decrease in infectability of these cells by the VSV-G control pseudotype virus (Carthagena et al., 2008; Nakayama and Shioda, 2010; Stremlau et al., 2004). Flow cytometry analysis for ACE2 showed a high level of expression on ACE2.293T, an intermediate level on ACE2.A549, and a low to undetectable level on Vero, Vero E6, A549, CaCO$_2$, and Huh7 (Figure S1). The absence of detectable ACE2 on these cell lines suggests either that virus can use very small amounts of the receptor for entry, or that there is an alternative receptor. To test this hypothesis, we pretreated the cells with a blocking anti-ACE2 antibody prior to infection. The antibody largely blocked infection of ACE2.293T but had no effect on infection of Vero and the other cell lines, suggesting the presence of an alternative receptor (Figure 1G).

ACE2 Microbody Potently Inhibits SARS-CoV-2 S-Mediated Virus Entry

Soluble ACE2 and ACE2-Fc fusions have been shown to inhibit SARS-CoV-2 infection (Case et al., 2020; Kuba et al., 2010; Lei et al., 2020; Monteil et al., 2020; Qian and Hu, 2020; Wysocki et al., 2010). To increase the effectiveness of soluble ACE2 and improve therapeutic potential, we generated an ACE2-"microbody" in which the ACE2 ectodomain was fused to a single IgG CH3 domain of the IgG Fc region (Figure 2A). This domain contains the disulfide bonding cysteine residues of the IgG Fc that are required to dimerize the protein, which would serve to increase the ACE2 microbody avidity for ACE2. To prevent potential unwanted effects of the protein on blood pressure as a result of the catalytic activity of ACE2, we mutated H345, one of the key active site histidine residues of ACE2, to alanine, a mutation that has been shown to block catalytic activity (Guy et al., 2005). H345 lies underneath the spike protein interaction site and so was predicted not to interfere with spike protein binding (Figure 2B). For comparison, we constructed vector encoding soluble ACE2 without the IgG CH3. The proteins were purified from transfected 293T cells and purified to homogeneity by nickel-nitrilotriacetic acid (Ni-NTA) agarose affinity chromatography followed by size exclusion chromatography (Figure S2). The oligomerization state of the proteins was analyzed by SDS-PAGE under nonreducing and reducing conditions. Under reducing conditions, the ACE2 and ACE2.H345A microbody proteins and soluble ACE2 ran at 130 and 120 kDa, consistent with their calculated molecular mass (Figures 2C and S2). Under nonreducing conditions, the ACE2 microbody and ACE2.H345A microbody proteins ran at 250 kDa, consistent with dimers, while the soluble ACE2 ran as a monomer with a mass of 120 kDa (Figure 2C). Analysis of the proteins by size-exclusion chromatog-

raphy coupled with multi-angle light scattering (SEC-MALS) under nondenaturing conditions showed all three proteins to have a molecular mass consistent with dimers (Figure 2D). The mass of the ACE2 and ACE2.H345A microbody proteins was 218 and 230 kDa, respectively, while soluble ACE2 was 180 kDa. Taken together, the results suggest that the ACE2 microbody proteins are disulfide-bonded dimers, whereas soluble ACE2 is a nondisulfide-bonded dimer.

ACE2 Microbody Binds to SARS-CoV-2 Pseudotyped Virus

To compare the relative ability of the soluble ACE2 proteins with virions that display the spike protein, we established a virion pull-down assay. Ni-NTA beads were incubated with a serial dilution of the carboxy-terminal His-tagged soluble ACE2 proteins. Free spike protein was removed, and the beads were then incubated with a fixed amount of lentiviral pseudotyped virions. Free virions were removed, and the bound virions were quantified by immunoblot analysis for virion p24 capsid protein. To confirm that virus binding to the beads was specific for the bead-bound ACE2, we tested control virions lacking the spike. The results showed that spike protein pseudotyped virions bound to the beads, while virions that lacked the spike protein failed to bind, confirming that the binding was specific (Figure 3A). In addition, a high-titer human serum from a recovered individual blocked binding of the virions to the bead-bound ACE2 microbody (Figure S5). Analysis of the soluble ACE2 and ACE2 microbody proteins that had bound to the beads showed that similar amounts of each protein had bound (Figure 3B). Immunoblot analysis of virion binding to the bead-bound soluble ACE2 proteins showed that the wild-type and H345A microbody proteins both bound to virions more efficiently than soluble ACE2 (Figure 3C), and that the ACE2.H345A microbody bound more virions than the wild-type microbody protein. This was unexpected because H345 does not lie in the interaction surface with the spike protein.

ACE2 Microbody Blocks SARS-CoV-2 Pseudotyped Virus Infection

To determine the relative antiviral activity of soluble ACE2 and the ACE2 microbody proteins, we tested their ability to block the infection SARS-CoV-2 Δ19 spike protein pseudotyped GFP/luciferase reporter virus. A fixed amount of pseudotyped reporter virus was incubated with the ACE2 proteins and then used to infect ACE2.293T cells. After 2 days, luciferase activity and the number of GFP$^+$ cells in the infected cultures were analyzed. For comparison, a high-titered recovered patient serum with a neutralizing titer of 1:330 (Figure S5) was also tested. The results showed that soluble ACE2 had moderate inhibitory activity with an EC$_{50}$ of 1.24 μg/mL. The ACE2 microbody was significantly more potent with an EC$_{50}$ of 0.36 μg/mL, and the ACE2.H345A microbody protein was somewhat more potent than the wild-type ACE2 microbody with an EC$_{50}$ of 0.15 μg/mL (Figure 4A). Inhibition of infection by the soluble ACE2 proteins was comparable with recovered patient serum, although it is not possible to directly compare the two inhibitors because the mass amount of anti-spike protein antibody in the serum is not known. To confirm the results, we analyzed the infected cells by flow cytometry to determine the number of GFP$^+$ cells. The inhibition curves
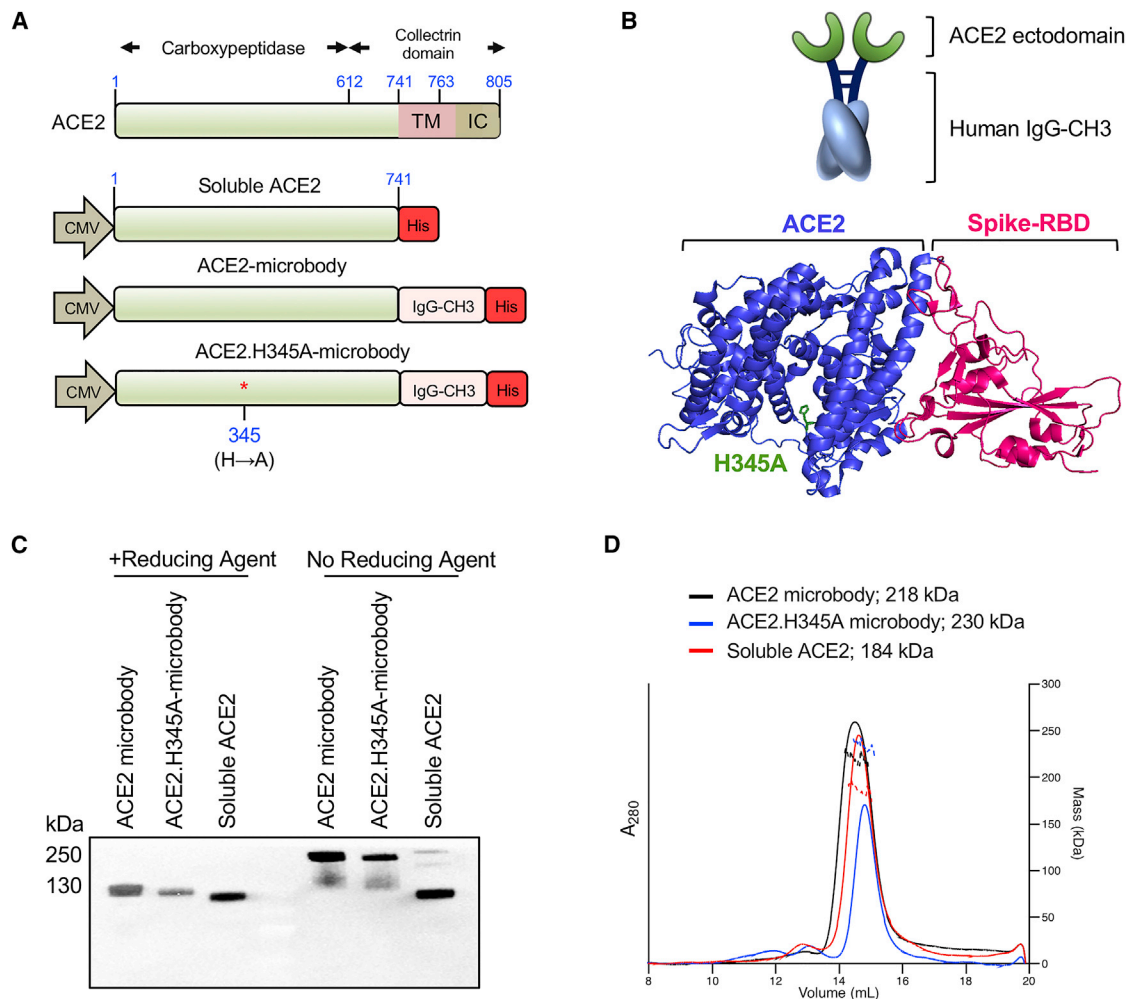
Figure 2. Wild-Type and H345A ACE2 Microbody Proteins Are Disulfide-Bonded Dimers

(A) The domains of ACE2 are shown with the structures of the soluble ACE2 (sACE2), ACE2 microbody, and ACE2.H345A microbody proteins below. The soluble ACE2 proteins are deleted for the transmembrane (TM) and cytoplasmic domains. The ACE2 microbody proteins are fused to the human IgG CH3 domain each with a carboxy-terminal 8× His-tag.

(B) The diagram above shows the predicted dimeric structure of the ACE2 microbody protein. The 3D structure of the ACE2:spike protein complex was generated using Chimera software (Pettersen et al., 2004) using published coordinates (Lan et al., 2020). The position of the conserved active site H345 in the ACE2 carboxypeptidase domain is shown lying underneath the ACE2 interaction site.

(C) 293T cells were transfected with sACE2, ACE2 microbody, and ACE2.H345A microbody expression vectors. The proteins were pulled down on NTA agarose beads and analyzed under reducing and nonreducing conditions on an immunoblot probed with anti-His-tag antibody.

(D) The soluble ACE2 proteins were purified by metal chelate chromatography and size exclusion chromatography (SEC). The oligomerization state was determined by SEC multi-angle light scattering. The calculated molecular mass of each is shown. The experiment was done twice with similar results.

were similar to the luciferase curves, confirming that the ACE2 proteins had decreased the number of cells infected and did not simply reduce expression of the reporter protein (Figure 4B, top). Representative images of the GFP+ cells provide visual confirmation of the results (Figure 4B, below). The inhibitory activity of the soluble ACE2 proteins was specific for the SARS-CoV-2 spike protein because they did not inhibit VSV-G pseudotyped virus (Figure 4C). The ACE2 microbody was somewhat more active when tested on untransfected 293T that express low levels of ACE2 (Figure 4D).

To determine the ability of the ACE2 microbody proteins to block the replication of live SARS-CoV-2, we used the replication-competent SARS-CoV-2, icSARS-CoV-2mNG, that encodes an mNeonGreen reporter gene in ORF7 (Xie et al., 2020). Serially diluted ACE2 microbody proteins were incubated with the virus, and the mixture was then used to infect ACE2.293T cells. The results showed that 1 to 0.125 μg of ACE2 microbody protein blocked live virus replication (Figure 4E). Soluble ACE2 was less active: 1 μg of the protein had a 50% antiviral effect, and the activity was lost with 0.5 μg. The antiviral activity of ACE2 proteins against live virus was similar to pseudotyped virus, except that in the live virus assay, the wild-type and H345A microbodies were of similar potency.
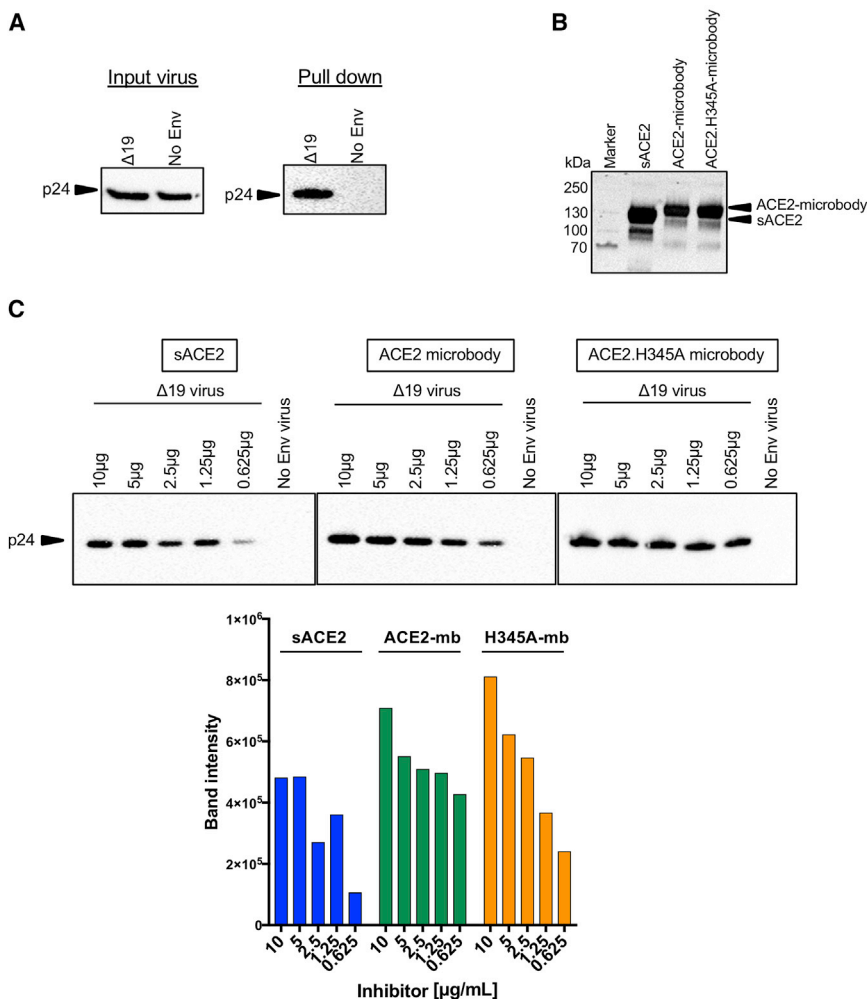
A

B

C

Figure 3. ACE2 Microbody Proteins Bind with High Affinity to SARS-CoV-2 S Pseudo-typed Virions

Nickel agarose beads were coated for 1 h with 10 μg of soluble ACE2 proteins. Unbound protein was removed, and SARS-CoV-2 Δ19 S pseudo-typed virions or virions lacking spike protein were incubated with the beads. After 1 h, unbound virions were removed, and the bound virions were analyzed on an immunoblot probed with anti-p24 antibody.

(A) Input virions and bead-bound virions were analyzed on an immunoblot probed with anti-p24 antibody.

(B) Soluble ACE2 proteins bound to the nickel agarose beads were analyzed on an immunoblot probed with anti-His-tag antibody.

(C) Soluble ACE2, wild-type ACE2 microbody, and ACE2.H345A microbody proteins were serially diluted and bound to nickel agarose beads. The amount of bound virions was determined by immunoblot analysis with anti-p24 antibody. Quantification of the band intensities from the immunoblot is graphed below for soluble ACE2 (sACE2), wild-type ACE2 microbody (ACE2-mb), and ACE2.H345A microbody (H345A-mb). The experiment was done twice with similar results.

In the experiments described above, the proteins were incubated with virus prior to infection. To determine whether they would be active at later time points, the ACE2 proteins were tested in an "escape from inhibition" assay in which the soluble ACE2 and ACE2 microbody proteins were added to cells at the same time as virus or up to 6 h post-infection. The results showed that addition of the microbody together with the virus (t_0) blocked the infection by 80%. Addition of the microbody 30 min post-infection maintained most of the antiviral effect, and even 2 h post-infection the inhibitor blocked 55% of the infection. At 4 h post-infection, the ACE2 microbody retained its blocking activity at 10 μg/mL but was less active with decreasing amounts of inhibitor (Figure 5A). These results suggest that the ACE2 microbody is highly efficient at neutralizing the virus when present before the virus has had a chance to bind to the cell, and that it maintains its ability to block infection when added together with the cells and even 2 h after the virus has been exposed to cells, a time at which most of the virus has not yet bound to the cell.

To determine whether the ACE2 microbody could prevent virus entry once the virus bound to the cell, the virus was prebound by incubating it with cells for 2 h at 22°C, the unbound virus was removed, and the ACE2 microbody was added at increasing time points. The results showed that removal of the unbound virus after 1-h incubation resulted in less infection as compared with when the virus was incubated with the cells for 4 h, indicating that only a fraction of the virus had bound to cells. However, virus that was bound could be blocked by the ACE2 microbody for another 30 min post-binding (Figure 5B). The ability to block entry of the cell-bound virus suggests that virus binding results from a small number of spike molecules binding to ACE2. Over the next 30–60 min, additional spike protein/ACE2 interactions form, escaping the ability of the ACE2 microbody to block virus entry. The results demonstrate that the ACE2 microbody is a highly potent inhibitor of free virus and maintains its antiviral activity against virus newly bound to the cell.

ACE2 Microbody Blocks Entry of Virus with D614G Spike

A variant SARS-CoV-2 containing a D614G point mutation in the spike protein has been found to be circulating in the human population with increasing prevalence (Daniloski et al., 2020; Eaaswarkhanth et al., 2020; Korber et al., 2020). The D614G mutation was found to decrease shedding of the spike protein from the virus and to assume a fusion-ready conformation, resulting in increased infectivity and most likely contributing to its increasing prevalence (Daniloski et al., 2020; Ozono et al., 2020; Zhang et al., 2020). To determine the ability of the soluble ACE2 proteins to block entry of virus with the D614G spike protein, we
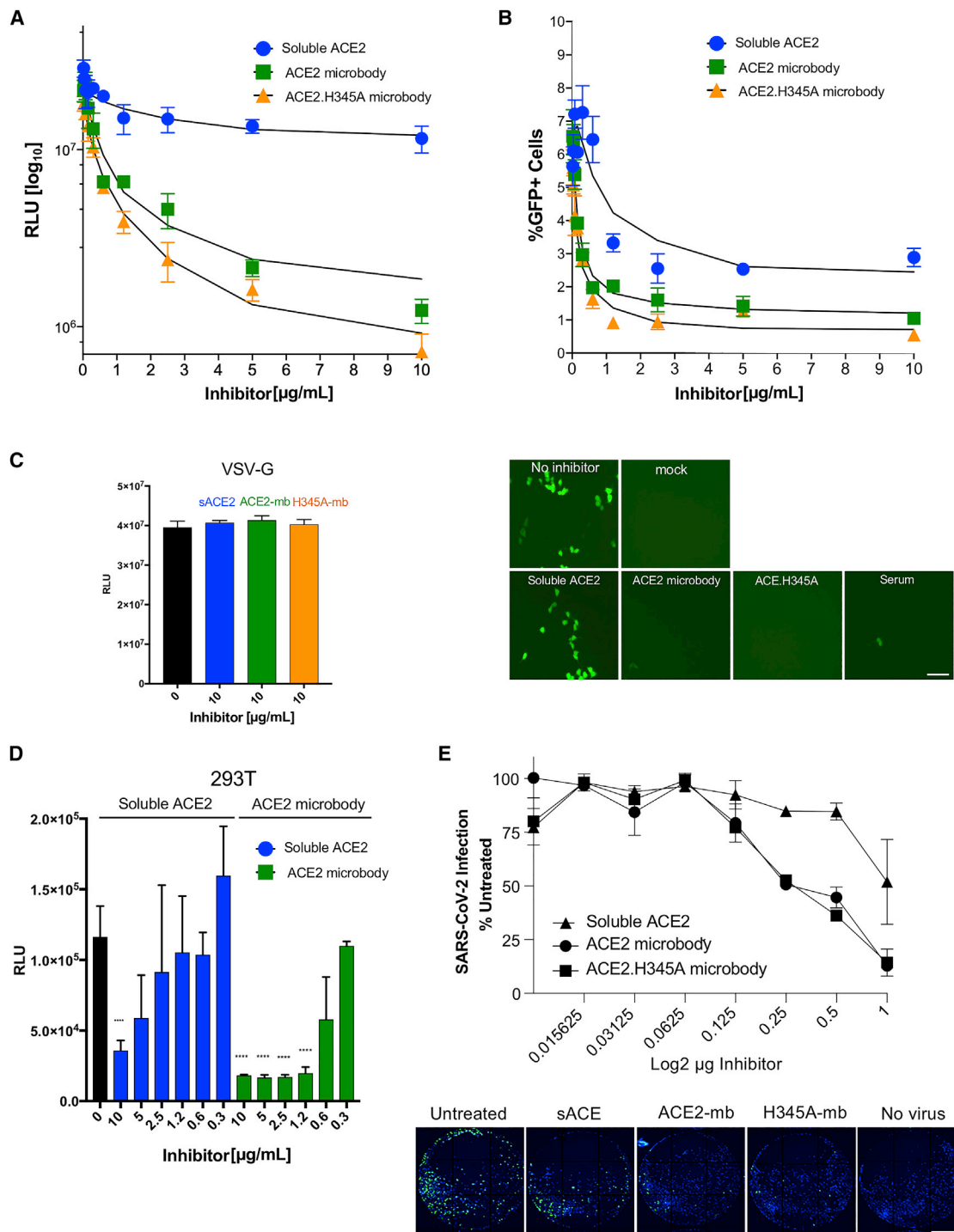
Figure 4. ACE2 and ACE2.H345A Microbodies Potently Block Virus Entry and Are Active on Different Cell Lines

(A) Serially diluted soluble ACE2, ACE2, and ACE2.H345A microbody proteins were incubated for 30 min with SARS-CoV-2 Δ19.S pseudotyped virus and then added to ACE2.293T cells. Luciferase activity was measured 2 days post-infection.

(B) The number of cells infected was determined by flow cytometry to quantify the GFP+ cells. The data are displayed as the percent of GFP+ cells. Representative fluorescence microscopy images of the infected cells are shown below. Scale bar, 50 μm.

(C) VSV-G pseudotyped lentiviral virions were incubated for 30 min with 10 μg/mL soluble ACE2 proteins and then added to ACE2.293T cells. Luciferase activity was measured 2 days post-infection.

(D) Δ19 spike protein pseudotyped virus was incubated with serially diluted soluble ACE2 proteins for 30 min and then added 293T cells.

introduced the mutation into the Δ19 spike protein expression vector and generated pseudotyped reporter viruses (Figure 6A). Analysis of the infectivity of the D614G and wild-type pseudotyped viruses on the panel of cell lines showed that the mutation increased the infectivity of virus 2- to 4-fold on 293T, ACE2.293T, Vero, and VeroE6 cells, consistent with previous reports (Daniloski et al., 2020; Ozono et al., 2020; Zhang et al., 2020). Infectivity of the mutated virus was also increased in A549, ACE2.A549 CaCO_2, although the overall infectivity of these cells was low (Figure 6B). To determine the ability of the soluble ACE2 proteins to neutralize the virus with the variant spike protein, we tested serial dilutions of the soluble ACE2 proteins for their ability to block wild-type and D614G S pseudotyped virus. The results showed that soluble ACE2 had moderate antiviral activity against wild-type virus, whereas the wild-type and H345A microbody proteins were more potent (Figure 6C). The ACE2.H345A microbody was more active at low concentration than the wild-type protein. To test the relative binding affinities of the soluble ACE2 proteins for the wild-type and D614G spike proteins, we used an ACE2/virion binding assay in which the soluble ACE2 proteins were bound to nickel beads via their His-tag (Figure 6D). Different amounts of wild-type or D614G pseudotyped virions were then incubated with the beads, and the amount of virions bound was quantified by immunoblot analysis. The results showed that the wild-type and H345A microbody proteins bound more efficiently than soluble ACE2 to the spike protein, and that they bound well to both the wild-type and D614G spike protein pseudotyped virions.

ACE2 Microbody Neutralizes Viruses with Other β Coronavirus Spike Proteins

To determine how well the ACE2 microbody would block the entry of other β coronaviruses, we generated lentiviral virions pseudotyped by spike proteins from a panel of different lineage 2 β coronaviruses that use ACE2 for entry (Letko and Munster, 2020) (pcSARS-CoV, pcSARS-CoV2, pcWIV1, pcLYRa11, pcRs4231, pcRs4084, and pcSHC014). The pseudotypes were incubated with soluble ACE2, and the ACE2 microbody proteins and their infectivity were then measured on ACE2.293T cells. The analysis showed that the ACE2 and H345A microbody proteins blocked all of the β coronavirus pseudotyped viruses, while the antiviral activity of soluble ACE2 was significantly diminished in comparison (Figure 6E). The results demonstrate the broad activity of the ACE2 microbody.

ACE2 Microbody Prevents Infection in a SARS-CoV-2 Mouse Model

K18-hACE2 transgenic mice express human ACE2 in epithelial airway cells (McCray et al., 2007). Infection of the mice with SARS-CoV2 by intranasal (i.n.) challenge results in virus replication that is first detected at day 2 in the lung and brain. The mice begin to lose weight at days 2–4 and die of the inflammatory response at days 6–9 (Hassan et al., 2020; Winkler et al.,

2020). To test the ability of the ACE2 microbody to prevent SARS-CoV-2 replication *in vivo*, we incubated live virus with the ACE2.H345 microbody protein, or buffer, and then administered the virus i.n. Mice infected with the buffer control-treated virus lost weight at day 2, whereas mice treated with the ACE2.H345A microbody showed no significant weight loss (Figure 7A). The control mice succumbed to the infection on day 6 post-infection, whereas mice treated with the ACE2.H345A microbody remained viable and healthy (Figure 7B). The results suggest that the microbody protein is able to prevent lethal SARS-CoV-2 disease *in vivo*.

DISCUSSION

We report the development of a soluble form of ACE2 in which the ectodomain of ACE2 is fused to a single domain of the IgG heavy chain Fc. The domain renders the protein smaller than those fused to the full-length Fc, yet retains the cysteine residues required for dimerization and the ability to increase the *in vivo* half-life (Maute et al., 2015). The microbody protein is a disulfide-bonded dimer, in contrast with soluble ACE2 lacking the Fc domain, which is dimeric, but not nondisulfide bonded. Although both proteins are dimeric, the ACE2 microbody had about 10-fold more antiviral activity than soluble ACE2 and bound to virions with a >4-fold increased affinity. The ACE2.H345A microbody protected mice from i.n. SARS-CoV-2 infection in the K18-hACE2 model.

Although high-affinity neutralizing monoclonal antibodies against the virus are of great value in the treatment of COVID-19, soluble receptor proteins have advantageous features. The ACE2 microbody is fully of human origin, so it should be relatively non-immunogenic. In addition, the requirement that the spike protein maintain its affinity for ACE2 should make it difficult for the virus to evolve escape mutants despite its relatively high mutation rate, because decreased binding to the soluble receptor proteins would decrease viral fitness. The microbody was fully active against virus with the D614G spike protein, a variant of increasing prevalence with increased infectivity *in vitro* (Figure 6B), and was highly active against ACE2-specific spike proteins from other β coronaviruses.

It has been shown that a recombinant ACE2-Fc fusion caused a marked decrease in blood pressure in a mouse model (Liu et al., 2018). To prevent this unwanted effect in the ACE2 microbody proteins, we introduced an H345A mutation into the protein. The mutation changes one of the histidine residues in the active site that is essential for ACE2 carboxypeptidase activity without impairing its antiviral activity against SARS CoV-2 or other β coronavirus spike proteins. In some experiments, the ACE2.H345A microbody appeared to be more active than the wild-type protein, although the significance of this difference was unclear because the two proteins had similar activity in the live virus replication assay.

(E) Serially diluted soluble ACE2 proteins were incubated with mNeonGreen SARS-CoV-2 for 30 min and then added to ACE2.293T cells. After 24 h, the GFP$^+$ cells were counted. Fluorescent microscopy images of representative fields from wells treated with 1 μg soluble ACE2, and ACE2 microbody proteins are shown below. Scale bar, 2.1 mm. The data are displayed as the mean ± SD, and significance is determined by Student's t tests. The experiments in (A)–(D) were repeated four times, and the experiment in (E) was done twice.
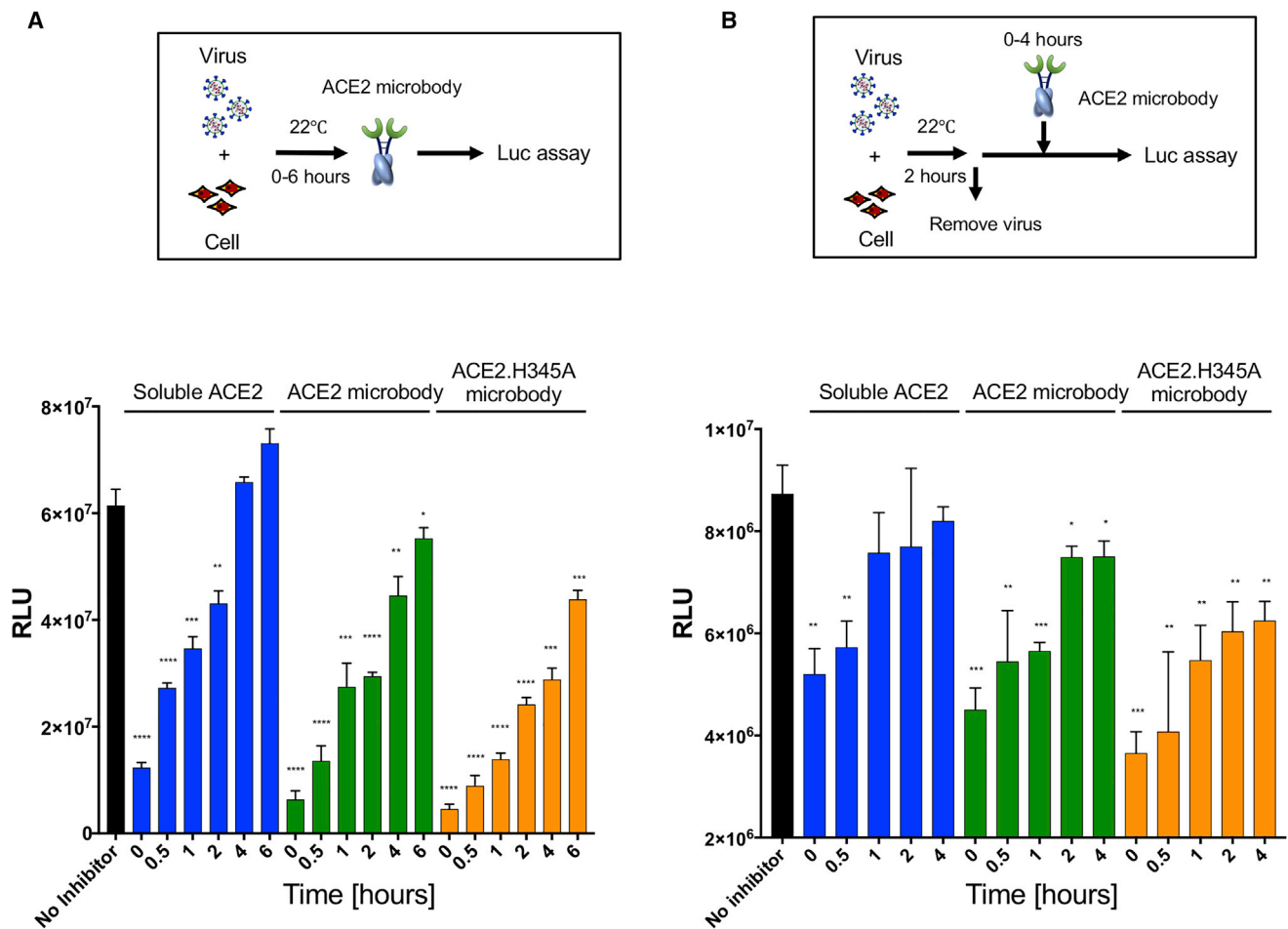
Figure 5. ACE2 Microbody Can Act after Virus/Cell Binding

The kinetics of ACE2 microbody inhibition were analyzed in an escape from inhibition assay.

(A) The experimental scheme is diagrammed above. SARS-CoV-2 Δ19.S pseudotyped virus was added to ACE2.293T cells. Soluble ACE2 proteins were added immediately or at time points up to 6 h later. Luciferase activity was measured 2 days post-infection.

(B) As diagrammed above, virus was bound to target cells for 2 h at 22°C, and unbound virus was then removed. Soluble ACE2 proteins were added as in (A). The data are displayed as the mean ± SD, and statistical significance was determined by Student's t tests. The experiment was done twice with similar results.

Escape from inhibition studies provided insight into the kinetics of virus infection and the mechanism of inhibition by the soluble receptors. Pretreatment of virus with the ACE2 microbody potently neutralized the virus, as did simultaneous addition of virus and microbody to cells. Furthermore, the protein retained its ability to prevent infection even when added to the culture at times after addition of virus, blocking infection by about 50% when added 1 h after virus addition. The ACE2 microbody was partially active even on virus that had already attached to the cell. When virus was pre-bound for 2 h, a time at which about 10% of the infectious virus had bound the cell, the ACE2 microbody retained the ability to prevent infection of about 50% of the bound virus (Figure 5A). Taken together, the experiments suggest a series of events in which the virus binds to cells over a period of about 4 h. During this time, the ACE2 microbody is highly efficient, neutralizing nearly all of the free virus. Once the virus binds to the cell, the ACE2 microbody retains its ability to block infection for about 30 min, suggesting that binding is

initially mediated by a small number of spike proteins, and that over 2 h additional spike proteins are recruited to interact with target cell ACE2, a period during which the ACE2 microbody remains able to block the viral fusion reaction. Once a sufficient number of spike protein/ACE2 interactions have formed, the virus escapes neutralization.

Because soluble ACE2 and the ACE2 microbody are both dimeric, it was surprising that the microbody had more antiviral activity. The ACE2 microbody protein also bound more efficiently to spike protein pseudotyped virions. The reasons for this difference are not clear. It is possible that the disulfide bonds of the ACE2 microbody stabilize the dimer, or that the individual monomers are positioned in a more favorable conformation to bind to the individual subunits of the spike protein trimer. Most of the experiments shown here used ACE2.293T cells that overexpress ACE2 as targets for infection. It is possible that the ACE2 microbody will have increased activity on cells that express ACE2 at physiological levels. Moreover, the ACE2 microbody protected
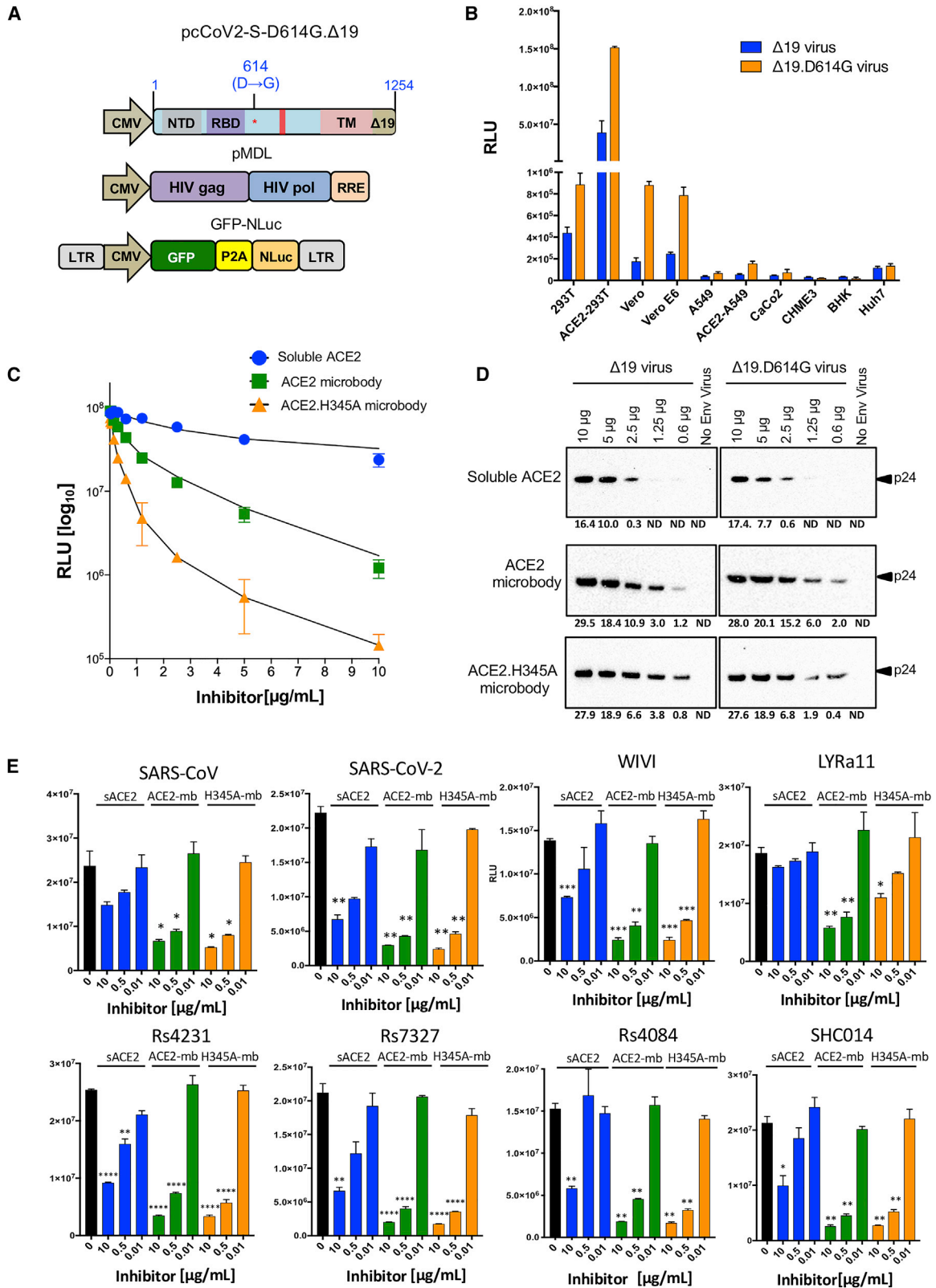
(legend on next page)

untransfected 293T cells that do not express ACE2 and are infected through an alternative receptor.

Recent reports have described similar soluble ACE2 proteins. Recently, soluble ACE2-related inhibitor including rhACE2 was shown to partially block infection (Case et al., 2020; Lei et al., 2020; Monteil et al., 2020), although the proteins had a short half-life (Wysocki et al., 2010) (<2 h in mice), limiting their clinical usefulness. In contrast, a dimeric rhesus ACE2-Fc fusion protein had a half-life in mice in plasma greater than 1 week (Liu et al., 2018). The half-life of the ACE2 microbody *in vivo* has not yet been tested, but the protein retained antiviral activity for several days in tissue culture, significantly longer than soluble ACE2 (Figure S3).

The phenomenon of antibody-dependent enhancement is caused by the interaction of the Fc domain of non-neutralizing antibody with the Fc receptor on cells, which then serves to promote rather than inhibit virus neutralization. A similar phenomenon is possible with receptor-Fc fusion proteins by interaction with Fc receptor on cells. Because the ACE2 microbody contained only a single Fc domain, it was not expected to interact with Fc receptor. To test whether this was the case, we tested the ACE2 microbody in an enhancement assay using U937 cells, which express Fc receptors. The ACE2 microbody protein did not detectably bind to cells that express the Fc γ receptor, and the cells did not become infected, suggesting that this mechanism is not likely to play a role *in vivo* (Figure S4 and data not shown).

SARS-CoV-2 pseudotyped lentiviruses have been developed by several laboratories as tools for titering neutralizing antibodies and testing entry inhibitors (Crawford et al., 2020; Nie et al., 2020; Ou et al., 2020; Schmidt et al., 2020; Shang et al., 2020; Xia et al., 2020). The pseudotyped lentiviral vector system we developed here is highly effective. The high infectivity of the viruses produced is due, in part, to codon optimization of the spike protein and to the cytoplasmic tail truncation. The Δ19 truncated spike protein was present at only slightly higher levels on the cell surface than the full-length protein, but it was packaged 20-fold more efficiently. A possible explanation for the increased packaging efficiency is that the full-length cytoplasmic tail sterically hinders virion incorporation by conflicting with the underlying viral matrix protein. Also contributing to high viral titers is the use of separate Gag/Pol packaging vector and lentiviral transfer vector as opposed to a lentiviral proviral DNA encoding Gag/Pol and the reporter gene, which we have found resulted in much

higher viral titer (data not shown). The use of a dual nanoluciferase/GFP reporter in the system allows for measurement of infectious virus titer by flow cytometry and highly sensitivity nanoluciferase readout. The results obtained using the lentiviral pseudotypes accurately reflect the results derived using live SARS-CoV-2. In a study of sera from over 100 convalescent patients, the pseudotype assay results were closely correlated with titers determined in a live virus neutralization assay (Noval et al., 2020).

In a survey of a panel of cell lines for susceptibility to infection by the spike protein pseudotyped virus that included several of those in use for SARS-CoV-2 studies, none was anywhere near as infectable as the ACE2.293T cells and did not express detectable levels of ACE2. For example, Vero E6 and $CaCO_2$ are highly susceptible to SARS-CoV-2 (Hoffmann et al., 2020) but were poorly infected by spike protein pseudotype virus (Figure 1F) and did not express detectable ACE2 (Figure S1), raising the question of how the cells support SARS-CoV-2 replication. The finding that pretreatment with a blocking anti-ACE2 antibody did not block their infection suggests that the cells are infected through an alternative receptor. Although the postulated receptor supports only inefficient virus entry, it is sufficient to support robust virus replication. Recent reports have suggested alternative receptors (Cantuti-Castelvetri et al., 2020; Davanzo et al., 2020), although whether these are expressed on the cell lines tested is not clear.

A feature of soluble receptors is that because the virus spike protein needs to conserve its receptor binding affinity, they should maintain their ability to neutralize spike protein variants. SARS-CoV-2 S variants have been found to circulate in the human population, and it is likely that others are yet to emerge, some of which may be less sensitive to neutralization by the therapeutic monoclonal antibodies currently under development. SARS-CoV-2 encoding the D614G spike protein has increased its frequency in the human population (Daniloski et al., 2020; Eaaswarkhanth et al., 2020; Korber et al., 2020). The D614G spike protein was found to be more resistant to shedding from the virion, adopting a conformation that favors ACE2 binding and lowers the energy barrier to cell fusion (Daniloski et al., 2020; Ozono et al., 2020; Zhang et al., 2020). The ACE2 microbody maintained its ability to neutralize D614G spike protein pseudotyped virus and was able to neutralize diverse β coronaviruses. The ACE2 microbody and similar soluble receptor proteins could be valuable tools able to neutralize coronaviruses

Figure 6. ACE2 Microbody Blocks Entry of the D614G Variant Spike Protein Pseudotyped Virus Infection and ACE2 Using β Coronavirus Spike Proteins

(A) The domain structure of the SARS-CoV-2 D614G Δ19 S expression vector is diagrammed above. Red star indicates the D614G mutation in the spike protein.

(B) A panel of cell lines was infected with equivalent amounts (MOI = 0.2) of wild-type and D614G Δ19 spike protein pseudotyped virus.

(C) Serially diluted soluble ACE2 and ACE2 microbody proteins were mixed with D614G Δ19 spike protein pseudotyped virus and added to target cells. Luciferase activity was measured 2 days post-infection. The data are shown as the mean of triplicates ± SD. The statistical significance of the data was calculated with the Student's t test.

(D) Ni-NTA agarose beads were coated with serially diluted soluble ACE2 and ACE2 microbody proteins. Wild-type, Δ19 spike protein, and no Env pseudotyped virions (28.2 ng p24) were added and allowed to bind. Unbound virions were removed after 30 min, and the bound virions were detected by immunoblot analysis with anti-p24 antibody. The amount (ng) of bead-bound virus p24 was calculated based on band intensities from the immunoblot and indicated in the bottom side.

(E) Lentiviral virions pseudotyped by β coronavirus lineage 2 spike proteins were treated with serially diluted soluble ACE2 proteins and then used to infect ACE2.293T cells. The identity of the virus from which the spike protein RBD is derived is indicated above each histogram. Luciferase activity was measured after 2 days. The data are displayed as the mean ± SD, and significance is determined by Student's t tests. The experiments in (B) and (C) were done three times, and those in (D) and (E) were done twice.
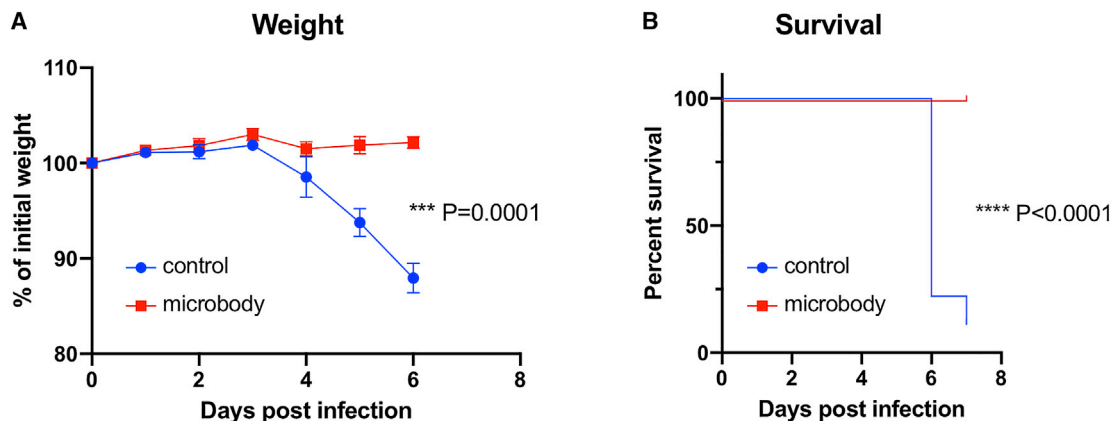
Figure 7. ACE2.H345A Microbody Protects K18-hACE2 Transgenic Mice from SARS-CoV-2 Infection
(A and B) ACE2.H345A microbody (7.5 μg) or control buffer was incubated for 30 min at room temperature with viral inoculum (1 × 10^3 plaque-forming units [PFUs] SARS-CoV-2). The virus was administered intranasally to K18h-ACE2 littermates (control: n = 9; microbody: n = 10), and the mice were then monitored for weight loss (A) and survival (B). Data are pooled from two independent experiments. Weight loss was analyzed by a mixed-effects model. Survival was analyzed by a log rank (Mantel-Cox) test. ****p < 0.0001.

that may be transferred to the human population in the future. Such soluble receptor proteins could serve as off-the-shelf reagents that could be rapidly deployed.

STAR★METHODS

Detailed methods are provided in the online version of this paper and include the following:

- KEY RESOURCES TABLE
- RESOURCE AVAILABILITY
  - Lead Contact
  - Materials Availability
  - Data and Code Availability
- EXPERIMENTAL MODEL AND SUBJECT DETAILS
  - Mouse Care and *In Vivo* SARS-CoV-2 Neutralization
  - Plasmids
  - Human Sera
  - Cells
- METHOD DETAILS
  - SARS-CoV-2 Lentiviral Pseudotype Assay
  - Protein Purification and Molecular Mass Determination
  - Virion Pull-Down Assay
  - Immunoblot Analysis
  - Binding Assay
  - Live SARS-CoV-2 Neutralization Assay
- QUANTIFICATION AND STATISTICAL ANALYSIS

SUPPLEMENTAL INFORMATION

Supplemental Information can be found online at https://doi.org/10.1016/j.celrep.2020.108528.

AUTHOR CONTRIBUTIONS

Conceptualization and Methodology, T.T., N.R.L., C.M.N., and C.B.W.; Investigation, T.T., C.F., J.S.C., R.K., K.A.S., H.G., and B.M.D.; Writing – Original Draft, T.T.; Writing – Review & Editing, N.R.L.; Funding Acquisition, N.R.L., C.M.N., C.B.W.; Resources, N.R.L., C.M.N., and C.B.W.; and Supervision, N.R.L.

DECLARATION OF INTERESTS

A provisional patent application has been filed with the US Patent and Trademark Office.

REFERENCES

Belouzard, S., Millet, J.K., Licitra, B.N., and Whittaker, G.R. (2012). Mechanisms of coronavirus cell entry mediated by the viral spike protein. Viruses *4*, 1011–1033.

Campeau, E., Ruhl, V.E., Rodier, F., Smith, C.L., Rahmberg, B.L., Fuss, J.O., Campisi, J., Yaswen, P., Cooper, P.K., and Kaufman, P.D. (2009). A versatile viral system for expression and depletion of proteins in mammalian cells. PLoS ONE *4*, e6529.

Cantuti-Castelvetri, L., Ojha, R., Pedro, L.D., Djannatian, M., Franz, J., Kuivanen, S., van der Meer, F., Kallio, K., Kaya, T., Anastasina, M., et al. (2020). Neuropilin-1 facilitates SARS-CoV-2 cell entry and infectivity. Science *370*, 856–860.

Carthagena, L., Parise, M.C., Ringeard, M., Chelbi-Alix, M.K., Hazan, U., and Nisole, S. (2008). Implication of TRIM alpha and TRIMCyp in interferon-induced anti-retroviral restriction activities. Retrovirology *5*, 59.

Case, J.B., Rothlauf, P.W., Chen, R.E., Liu, Z., Zhao, H., Kim, A.S., Bloyet, L.M., Zeng, Q., Tahan, S., Droit, L., et al. (2020). Neutralizing antibody and soluble ACE2 inhibition of a replication-competent VSV-SARS-CoV-2 and a

clinical isolate of SARS-CoV-2. bioRxiv. https://doi.org/10.1101/2020.05.18.102038.

Chiang, J.J., Gardner, M.R., Quinlan, B.D., Dorfman, T., Choe, H., and Farzan, M. (2012). Enhanced recognition and neutralization of HIV-1 by antibody-derived CCR5-mimetic peptide variants. J. Virol. 86, 12417–12421.

Crawford, K.H.D., Eguia, R., Dingens, A.S., Loes, A.N., Malone, K.D., Wolf, C.R., Chu, H.Y., Tortorici, M.A., Veesler, D., Murphy, M., et al. (2020). Protocol and Reagents for Pseudotyping Lentiviral Particles with SARS-CoV-2 Spike Protein for Neutralization Assays. Viruses 12, 513.

Daar, E.S., Li, X.L., Moudgil, T., and Ho, D.D. (1990). High concentrations of recombinant soluble CD4 are required to neutralize primary human immunodeficiency virus type 1 isolates. Proc. Natl. Acad. Sci. USA 87, 6574–6578.

Daniloski, Z., Guo, X., and Sanjana, N.E. (2020). The D614G mutation in SARS-CoV-2 Spike increases transduction of multiple human cell types. bioRxiv. https://doi.org/10.1101/2020.06.14.151357.

Davanzo, G.G., Codo, A.C., Brunetti, N.S., Boldrini, V.O., Knittel, T.L., Monterio, L.B., de Moraes, D., Ferrari, A.J.R., de Souza, G.F., Muraro, S.P., et al. (2020). SARS-CoV-2 Uses CD4 to Infect T Helper Lymphocytes. medRxiv, 2020.09.25.20200329.

Eaaswarkhanth, M., Al Madhoun, A., and Al-Mulla, F. (2020). Could the D614G substitution in the SARS-CoV-2 spike (S) protein be associated with higher COVID-19 mortality? Int. J. Infect. Dis. 96, 459–460.

Eroshenko, N., Gill, T., Keaveney, M.K., Church, G.M., Trevejo, J.M., and Rajaniemi, H. (2020). Implications of antibody-dependent enhancement of infection for SARS-CoV-2 countermeasures. Nat. Biotechnol. 38, 789–791.

Fehr, A.R., and Perlman, S. (2015). Coronaviruses: an overview of their replication and pathogenesis. Methods Mol. Biol. 1282, 1–23.

Giroglou, T., Cinatl, J., Jr., Rabenau, H., Drosten, C., Schwalbe, H., Doerr, H.W., and von Laer, D. (2004). Retroviral vectors pseudotyped with severe acute respiratory syndrome coronavirus S protein. J. Virol. 78, 9007–9015.

Glowacka, I., Bertram, S., Müller, M.A., Allen, P., Soilleux, E., Pfefferle, S., Steffen, I., Tsegaye, T.S., He, Y., Gnirss, K., et al. (2011). Evidence that TMPRSS2 activates the severe acute respiratory syndrome coronavirus spike protein for membrane fusion and reduces viral control by the humoral immune response. J. Virol. 85, 4122–4134.

Guy, J.L., Jackson, R.M., Jensen, H.A., Hooper, N.M., and Turner, A.J. (2005). Identification of critical active-site residues in angiotensin-converting enzyme-2 (ACE2) by site-directed mutagenesis. FEBS J. 272, 3512–3520.

Haim, H., Si, Z., Madani, N., Wang, L., Courter, J.R., Princiotto, A., Kassa, A., DeGrace, M., McGee-Estrada, K., Mefford, M., et al. (2009). Soluble CD4 and CD4-mimetic compounds inhibit HIV-1 infection by induction of a short-lived activated state. PLoS Pathog. 5, e1000360.

Harmer, D., Gilbert, M., Borman, R., and Clark, K.L. (2002). Quantitative mRNA expression profiling of ACE 2, a novel homologue of angiotensin converting enzyme. FEBS Lett. 532, 107–110.

Haschke, M., Schuster, M., Poglitsch, M., Loibner, H., Salzberg, M., Brug-gisser, M., Penninger, J., and Krähenbühl, S. (2013). Pharmacokinetics and pharmacodynamics of recombinant human angiotensin-converting enzyme 2 in healthy human subjects. Clin. Pharmacokinet. 52, 783–792.

Hassan, A.O., Case, J.B., Winkler, E.S., Thackray, L.B., Kafai, N.M., Bailey, A.L., McCune, B.T., Fox, J.M., Chen, R.E., Alsoussi, W.B., et al. (2020). A SARS-CoV-2 Infection Model in Mice Demonstrates Protection by Neutralizing Antibodies. Cell 182, 744–753.e4.

Heald-Sargent, T., and Gallagher, T. (2012). Ready, set, fuse! The coronavirus spike protein and acquisition of fusion competence. Viruses 4, 557–580.

Hoffmann, M., Kleine-Weber, H., Schroeder, S., Krüger, N., Herrler, T., Erichsen, S., Schiergens, T.S., Herrler, G., Wu, N.H., Nitsche, A., et al. (2020). SARS-CoV-2 Cell Entry Depends on ACE2 and TMPRSS2 and Is Blocked by a Clinically Proven Protease Inhibitor. Cell 181, 271–280.e8.

Khan, A., Benthin, C., Zeno, B., Albertson, T.E., Boyd, J., Christie, J.D., Hall, R., Poirier, G., Ronco, J.J., Tidswell, M., et al. (2017). A pilot clinical trial of recombinant human angiotensin-converting enzyme 2 in acute respiratory distress syndrome. Crit. Care 21, 234.

Korber, B., Fischer, W.M., Gnanakaran, S., Yoon, H., Theiler, J., Abfalterer, W., Hengartner, N., Giorgi, E.E., Bhattacharya, T., Foley, B., et al. (2020). Tracking Changes in SARS-CoV-2 Spike: Evidence that D614G Increases Infectivity of the COVID-19 Virus. Cell 182, 812–827.e19.

Ksiazek, T.G., Erdman, D., Goldsmith, C.S., Zaki, S.R., Peret, T., Emery, S., Tong, S., Urbani, C., Comer, J.A., Lim, W., et al.; SARS Working Group (2003). A novel coronavirus associated with severe acute respiratory syndrome. N. Engl. J. Med. 348, 1953–1966.

Kuba, K., Imai, Y., Rao, S., Gao, H., Guo, F., Guan, B., Huan, Y., Yang, P., Zhang, Y., Deng, W., et al. (2005). A crucial role of angiotensin converting enzyme 2 (ACE2) in SARS coronavirus-induced lung injury. Nat. Med. 11, 875–879.

Kuba, K., Imai, Y., Ohto-Nakanishi, T., and Penninger, J.M. (2010). Trilogy of ACE2: a peptidase in the renin-angiotensin system, a SARS receptor, and a partner for amino acid transporters. Pharmacol. Ther. 128, 119–128.

Lan, J., Ge, J., Yu, J., Shan, S., Zhou, H., Fan, S., Zhang, Q., Shi, X., Wang, Q., Zhang, L., and Wang, X. (2020). Structure of the SARS-CoV-2 spike receptor-binding domain bound to the ACE2 receptor. Nature 581, 215–220.

Lei, C., Qian, K., Li, T., Zhang, S., Fu, W., Ding, M., and Hu, S. (2020). Neutralization of SARS-CoV-2 spike pseudotyped virus by recombinant ACE2-Ig. Nat. Commun. 11, 2070.

Letko, M., and Munster, V. (2020). Functional assessment of cell entry and receptor usage for lineage B beta-coronaviruses, including 2019-nCoV. bioRxiv. https://doi.org/10.1101/2020.01.22.915660.

Leung, W.K., To, K.F., Chan, P.K., Chan, H.L., Wu, A.K., Lee, N., Yuen, K.Y., and Sung, J.J. (2003). Enteric involvement of severe acute respiratory syndrome-associated coronavirus infection. Gastroenterology 125, 1011–1017.

Li, F. (2015). Receptor recognition mechanisms of coronaviruses: a decade of structural studies. J. Virol. 89, 1954–1964.

Li, W., Moore, M.J., Vasilieva, N., Sui, J., Wong, S.K., Berne, M.A., Somasundaran, M., Sullivan, J.L., Luzuriaga, K., Greenough, T.C., et al. (2003). Angiotensin-converting enzyme 2 is a functional receptor for the SARS coronavirus. Nature 426, 450–454.

Li, F., Li, W., Farzan, M., and Harrison, S.C. (2005). Structure of SARS coronavirus spike receptor-binding domain complexed with receptor. Science 309, 1864–1868.

Li, W., Choe, H., and Farzan, M. (2006). Insights from the association of SARS-CoV S-protein with its receptor, ACE2. Adv. Exp. Med. Biol. 581, 209–218.

Liu, P., Wysocki, J., Souma, T., Ye, M., Ramirez, V., Zhou, B., Wilsbacher, L.D., Quaggin, S.E., Battle, D., and Jin, J. (2018). Novel ACE2-Fc chimeric fusion provides long-lasting hypertension control and organ protection in mouse models of systemic renin angiotensin system activation. Kidney Int. 94, 114–125.

Matsuyama, S., Nagata, N., Shirato, K., Kawase, M., Takeda, M., and Taguchi, F. (2010). Efficient activation of the severe acute respiratory syndrome coronavirus spike protein by the transmembrane protease TMPRSS2. J. Virol. 84, 12658–12664.

Maute, R.L., Gordon, S.R., Mayer, A.T., McCracken, M.N., Natarajan, A., Ring, N.G., Kimura, R., Tsai, J.M., Manglik, A., Kruse, A.C., et al. (2015). Engineering high-affinity PD-1 variants for optimized immunotherapy and immuno-PET imaging. Proc. Natl. Acad. Sci. USA 112, E6506–E6514.

McCray, P.B., Jr., Pewe, L., Wohlford-Lenane, C., Hickey, M., Manzel, L., Shi, L., Netland, J., Jia, H.P., Halabi, C., Sigmund, C.D., et al. (2007). Lethal infection of K18-hACE2 mice infected with severe acute respiratory syndrome coronavirus. J. Virol. 81, 813–821.

Monteil, V., Kwon, H., Prado, P., Hagelkrüys, A., Wimmer, R.A., Stahl, M., Leopoldi, A., Garreta, E., Hurtado Del Pozo, C., Prosper, F., et al. (2020). Inhibition of SARS-CoV-2 Infections in Engineered Human Tissues Using Clinical-Grade Soluble Human ACE2. Cell 181, 905–913.e7.

Nakayama, E.E., and Shioda, T. (2010). Anti-retroviral activity of TRIM5 alpha. Rev. Med. Virol. 20, 77–92.

Nie, J., Li, Q., Wu, J., Zhao, C., Hao, H., Liu, H., Zhang, L., Nie, L., Qin, H., Wang, M., et al. (2020). Establishment and validation of a pseudovirus neutralization assay for SARS-CoV-2. Emerg. Microbes Infect. 9, 680–686.

Noval, M.G., Kaczmarek, M.E., Koide, A., Rodriguez-Rodriguez, B.A., Louie, P., Tada, T., Hattori, T., Panchenko, T., Romero, L.A., Teng, K.W., et al. (2020). High titers of multiple antibody isotypes against the SARS-CoV-2 spike receptor-binding domain and nucleoprotein associate with better neutralization. bioRxiv. https://doi.org/10.1101/2020.08.15.252353.

Orloff, S.L., Kennedy, M.S., Belperron, A.A., Maddon, P.J., and McDougal, J.S. (1993). Two mechanisms of soluble CD4 (sCD4)-mediated inhibition of human immunodeficiency virus type 1 (HIV-1) infectivity and their relation to primary HIV-1 isolates with reduced sensitivity to sCD4. J. Virol. 67, 1461–1471.

Ou, X., Liu, Y., Lei, X., Li, P., Mi, D., Ren, L., Guo, L., Guo, R., Chen, T., Hu, J., et al. (2020). Characterization of spike glycoprotein of SARS-CoV-2 on virus entry and its immune cross-reactivity with SARS-CoV. Nat. Commun. 11, 1620.

Ozono, S., Zhang, Y., Ode, H., Tan, T.S., Imai, K., Miyoshi, K., Kishigami, S., Ueno, T., Iwatani, Y., Suzuki, T., and Tokunaga, K. (2020). Naturally mutated spike proteins of SARS-CoV-2 variants show differential levels of cell entry. bioRxiv. https://doi.org/10.1101/2020.06.15.151779.

Pettersen, E.F., Goddard, T.D., Huang, C.C., Couch, G.S., Greenblatt, D.M., Meng, E.C., and Ferrin, T.E. (2004). UCSF Chimera—a visualization system for exploratory research and analysis. J. Comput. Chem. 25, 1605–1612.

Qian, K., and Hu, S. (2020). Ig-like ACE2 protein therapeutics: A revival in development during the COVID-19 pandemic. MAbs 12, e1782600.

Riordan, J.F. (2003). Angiotensin-I-converting enzyme and its relatives. Genome Biol. 4, 225.

Schenten, D., Marcon, L., Karlsson, G.B., Parolin, C., Kodama, T., Gerard, N., and Sodroski, J. (1999). Effects of soluble CD4 on simian immunodeficiency virus infection of CD4-positive and CD4-negative cells. J. Virol. 73, 5373–5380.

Schmidt, F., Weisblum, Y., Muecksch, F., Hoffmann, H.H., Michailidis, E., Lorenzi, J.C.C., Mendoza, P., Rutkowska, M., Bednarski, E., Gaebler, C., et al. (2020). Measuring SARS-CoV-2 neutralizing antibody activity using pseudotyped and chimeric viruses. J. Exp. Med. 217, e20201181.

Shang, J., Wan, Y., Luo, C., Ye, G., Geng, Q., Auerbach, A., and Li, F. (2020). Cell entry mechanisms of SARS-CoV-2. Proc. Natl. Acad. Sci. USA 117, 11727–11734.

Shulla, A., Heald-Sargent, T., Subramanya, G., Zhao, J., Perlman, S., and Gallagher, T. (2011). A transmembrane serine protease is linked to the severe

acute respiratory syndrome coronavirus receptor and activates virus entry. J. Virol. 85, 873–882.

Stremlau, M., Owens, C.M., Perron, M.J., Kiessling, M., Autissier, P., and Sodroski, J. (2004). The cytoplasmic body component TRIM5alpha restricts HIV-1 infection in Old World monkeys. Nature 427, 848–853.

Sullivan, N., Sun, Y., Binley, J., Lee, J., Barbas, C.F., 3rd, Parren, P.W., Burton, D.R., and Sodroski, J. (1998). Determinants of human immunodeficiency virus type 1 envelope glycoprotein activation by soluble CD4 and monoclonal antibodies. J. Virol. 72, 6332–6338.

Tikellis, C., and Thomas, M.C. (2012). Angiotensin-Converting Enzyme 2 (ACE2) Is a Key Modulator of the Renin Angiotensin System in Health and Disease. Int. J. Pept. 2012, 256294.

Vermeire, J., Naessens, E., Vanderstraeten, H., Landi, A., Iannucci, V., Van Nuffel, A., Taghon, T., Pizzato, M., and Verhasselt, B. (2012). Quantification of reverse transcriptase activity by real-time PCR as a fast and accurate method for titration of HIV, lenti- and retroviral vectors. PLoS ONE 7, e50859.

Wei, J., Alfajaro, M.M., Hanna, R.E., DeWeirdt, P.C., Strine, M.S., Lu-Culligan, W.J., Zhang, S.M., Graziano, V.R., Schmitz, C.O., Chen, J.S., et al. (2020). Genome-wide CRISPR screen reveals host genes that regulate SARS-CoV-2 infection. bioRxiv. https://doi.org/10.1101/2020.06.16.155101.

Winkler, E.S., Bailey, A.L., Kafai, N.M., Nair, S., McCune, B.T., Yu, J., Fox, J.M., Chen, R.E., Earnest, J.T., Keeler, S.P., et al. (2020). SARS-CoV-2 infection of human ACE2-transgenic mice causes severe lung inflammation and impaired function. Nat. Immunol. 21, 1327–1335.

Wysocki, J., Ye, M., Rodriguez, E., González-Pacheco, F.R., Barrios, C., Evora, K., Schuster, M., Loibner, H., Brosnihan, K.B., Ferrario, C.M., et al. (2010). Targeting the degradation of angiotensin II with recombinant angiotensin-converting enzyme 2: prevention of angiotensin II-dependent hypertension. Hypertension 55, 90–98.

Xia, S., Liu, M., Wang, C., Xu, W., Lan, Q., Feng, S., Qi, F., Bao, L., Du, L., Liu, S., et al. (2020). Inhibition of SARS-CoV-2 (previously 2019-nCoV) infection by a highly potent pan-coronavirus fusion inhibitor targeting its spike protein that harbors a high capacity to mediate membrane fusion. Cell Res. 30, 343–355.

Xie, X., Muruato, A., Lokugamage, K.G., Narayanan, K., Zhang, X., Zou, J., Liu, J., Schindewolf, C., Bopp, N.E., Aguilar, P.V., et al. (2020). An Infectious cDNA Clone of SARS-CoV-2. Cell Host Microbe 27, 841–848.e3.

Zhang, L., Jackson, C.B., Mou, H., Ojha, A., Rangarajan, E.S., Izard, T., Farzan, M., and Choe, H. (2020). The D614G mutation in the SARS-CoV-2 spike protein reduces S1 shedding and increases infectivity. bioRxiv. https://doi.org/10.1101/2020.06.12.148726.

STAR★METHODS

KEY RESOURCES TABLE

REAGENT or RESOURCE	SOURCE	IDENTIFIER
Antibodies		
anti-HA antibody	Covance	Cat# MMS-101R; RRID:AB_291262
anti-His	Invitrogen	Cat# 372900; RRID:AB_2533309
anti-GAPDH	Life Technologies	Cat# AM4300; RRID:AB_2536381
anti-p24 antibody (AG3.0)	AIDS respository	Cat# 4121; RRID:AB_2734137
anti-ACE2 antibody (AC384)	NOVUS	Cat# NBP2-80038
Anti-spike antibody	GeneTex	Cat# GTX632604; RRID:AB_2864418
Alexa Fluor 594-conjugated goat anti-mouse IgG	Biolegend	Cat# 405326; RRID:AB_2563308
goat anti-mouse HRP-conjugated second antibody	Sigma	Cat# A4416; RRID:AB_258167
Bacterial and Virus Strains		
VSV-G pseudotyped reporter virus	This paper	N/A
SARS-CoV-2 full-length S pseudotyped reporter virus	This paper	N/A
SARS-CoV-2 Δ19 S pseudotyped reporter virus	This paper	N/A
SARS-CoV-2 Δ19 S D614G pseudotyped reporter virus	This paper	N/A
SARS-CoV pseudotyped reporter virus	This paper	N/A
WIV1 pseudotyped reporter virus	This paper	N/A
LYRa11 pseudotyped reporter virus	This paper	N/A
Rs4231 pseudotyped reporter virus	This paper	N/A
Rs4084 pseudotyped reporter virus	This paper	N/A
SHC014 pseudotyped reporter virus	This paper	N/A
mNeonGreen SARS-CoV-2	Xie et al. (2020), *Cell Host and Microbe*	N/A
SARS-CoV-2 isolate USA-WA1/2020	BEI Resources	Cat# NR-52281
Biological Samples		
convalescent sera	NYU Vaccine Center with written consent under I.R.B. approval	IRB 20-00595 and IRB 18-02037
Chemicals, Peptides, and Recombinant Proteins		
nevirapine	NYU Pharmacy	Cat# 4666
ACE2 microbody	This paper	N/A
ACE2.H345A microbody	This paper	N/A
Soluble ACE2	This paper	N/A
polyethyleneimine	Polysciences	Cat# 23966-1
Critical Commercial Assays		
GIBCO ExpiFectamine CHO Transfection Kits	Thermo Fisher Scientific	Cat# A29130
Nano-Glo® Luciferase Assay System	Promega	Cat# N1120
Nickel-nitrilotriacetic acid-agarose beads	QIAGEN	Cat# D-40724
Dawn Heleos II 18-angle light-scattering detector	Wyatt Technology	https://www.wyatt.com/products/instruments/dawn-multi-angle-light-scattering-detector.html
Dynamic light-scattering detector	Wyatt Technology	https://www.wyatt.com/products/instruments/dynamic-electrophoretic-light-scattering-detectors.html
Optilab t-rEX refractive index detector	Wyatt Technology	Cat# Optilab T-rEX

(Continued on next page)

Continued

REAGENT or RESOURCE	SOURCE	IDENTIFIER
Experimental Models: Cell Lines		
293T	ATCC	N/A
ACE2.293T	This paper	N/A
Vero	ATCC	N/A
Vero E6	ATCC	N/A
CaCO2	ATCC	N/A
A549	Benjamin tenOever (ISMMS)	N/A
ACE2.A549	This paper	N/A
BHK	ATCC	N/A
Huh7	ATCC	N/A
CHME3	ATCC	N/A
U937	ATCC	N/A
CHO	Thermo Fisher	Cat# A29130
293F	Thermo Fisher	Cat# R79007
Experimental Models: Organisms/Strains		
K18-hACE2 mice [B6.Cg-Tg(K18-ACE2)2Prlmn/J	Jackson Laboratory	Stock No: 034860
Oligonucleotides (5''-3'')		
See Table S1 for primers	IDT	This paper
Recombinant DNA		
S fragment A (cDNA). See Table S2 for sequence	Thermo Fisher	This paper
S fragment B (cDNA). See Table S2 for sequence	Thermo Fisher	This paper
ACE2 (cDNA). See Table S2 for sequence	Origene	This paper
pLenti.CMV.GFP.puro	Addgene	Cat# 17448
Software and Algorithms		
MacVector ver 17.0.0 (27)	MacVector Inc	N/A
GraphPad Prism 7 7.0e Software	GraphPad Prism Software, Inc.	N/A
FlowJo 10.5.3	FlowJo, LLC	N/A
ASTRA 6 software	Wyatt Technology	N/A

RESOURCE AVAILABILITY

Lead Contact
Further information and requests for resources and reagents should be directed to and will be fulfilled by the Lead Contact, Nathaniel R. Landau (nathaniel.landau@med.nyu.edu).

Materials Availability
All unique DNA constructs, proteins, and pseudotyped virus generated in this study are available from the Lead Contact upon request.

Data and Code Availability
Additional supplemental items are available at Mendeley Data: http://doi.org/10.17632/hsbn73xpkt.1.

EXPERIMENTAL MODEL AND SUBJECT DETAILS

Mouse Care and *In Vivo* SARS-CoV-2 Neutralization
K18-hACE2 mice [B6.Cg-Tg(K18-ACE2)2Prlmn/J (McCray et al., 2007)] were purchased from The Jackson Laboratory and bred in-house. Mice of both sexes between 6 and 8 weeks old were used for this study. SARS-CoV-2 stock was generated as previously described (Wei et al., 2020). Briefly, a SARS-CoV-2 P1 stock was generated by inoculating Vero E6 cells with SARS-CoV-2 isolate USA-WA1/2020 (BEI Resources, NR-52281). The P1 stock was then used to inoculate Vero E6 cells at a MOI 0.01. After three days, the supernatant was harvested, clarified by centrifugation at 450 X g for 5 minutes, filtered through a 0.45-micron filter and stored in aliquots at $-80°C$. Infectious titer of the virus determined by plaque assay on Vero.E6 cells (Wei et al., 2020). SARS-CoV-2 (2.0 X 10⁴

PFU/ml) was mixed with ACE2 microbody (150 μg/ml) or buffer control and incubated for 30 minutes at room temperature. K18-hACE2 mice were anesthetized with 30% vol/vol isoflurane diluted in propylene glycol and administered 50 μl of the mixture (1 X 10^3 PFU SARS-CoV-2 + 7.5 μg ACE2 microbody or volume-matched buffer control) intranasally. The mice were weighed and monitored daily for survival. Littermate controls were used for all experiments. Animal use and care was approved in agreement with the Yale Animal Resource Center and Institutional Animal Care and Use Committee (#2018-20198) according to the standards set by the Animal Welfare Act.

Plasmids
The dual GFP/nanoluciferase lentiviral vector pLenti.GFP.NLuc was generated by overlap extension PCR. A DNA fragment encoding GFP was amplified with a forward primer containing a BamH-I site and a reverse primer encoding the P2A sequence. The nanoluciferase gene (NLuc) was amplified with a forward primer encoding the P2A motif and a reverse primer containing a 3′-Sal-I site. The amplicons were mixed and amplified with the external primers. The fused amplicon was cleaved with BamH-I and Sal-I and cloned into pLenti.CMV.GFP.puro (Addgene plasmid #17448, provided by Eric Campeau and Paul Kaufman) (Campeau et al., 2009).

The SARS-CoV-2 S expression vector pcCOV2.S was chemically synthesized as DNA fragments A and B encoding codon-optimized 5′ and 3′ halves, respectively, of the S gene of Wuhan-Hu-1/2019 SARS-CoV-2 isolate (Tables S2 and S3). Fragment A was amplified with a forward primer containing a Kpn-I site and reverse primer containing an EcoR-I site. The amplicon was cleaved with Kpn-I and EcoR-I and cloned into pcDNA6 (Invitrogen). Fragment B was amplified with a forward primer containing an EcoR-I site and reverse primer containing Mlu-I and Xho-I sites. The amplicon was cleaved with EcoR-I and Xho-I and cloned into pcDNA6. The cloned fragment A was then cleaved with Mlu-I and Xho-I and cloned into the Mlu-I and Xho-I sites in the fragment B-containing plasmid. To generate the SARS-CoV-2 S Δ19 expression vector pcCoV2.S.Δ19, the codon-optimized S gene was amplified with a forward primer containing a Kpn-I site and reverse primer that deleted the 19 carboxy-terminal amino acids and contained an Xho-I site. The amplicon was cloned into the Kpn-I and Xho-I of pcDNA6. The D614G mutation in S was generated by overlap extension PCR of the Δ19 S gene using internal primers overlapping the sequence encoding D614G and cloned into pcDNA6. Beta coronavirus spike expression vectors (Letko and Munster, 2020) (pcSARS-CoV, pcSARS-CoV2, pcWIV1, pcLYRa11, pcRs4231, pcRs4084 and pcSHC014) were kindly provided by Michael Letko and Vincent Munster (NIH).

ACE2 expressing lentiviral vector pLenti.ACE2 was generated by amplifying an ACE2 cDNA (Origene) with a forward primer containing an Xba-I site and reverse primer containing a Sal-I site. The amplicon was cleaved with Xba-I and Sal-I and cloned into pLenti.CMV.GFP.puro in place of GFP. The soluble ACE2 expression vector pcsACE2 was generated by amplifying the extracellular domain of ACE2 with a forward primer containing a Kpn-I site and reverse primer encoding an in-frame 8XHis-tag and Xho-I site. The amplicon was then cloned into the Kpn-I and Xho-I sites of pcDNA6. The ACE2 microbody expression vector pcACE2-microbody was generated by overlap extension PCR that fused the extracellular domain of ACE2 with human immunoglobulin G heavy chain Fc domain 3 using a forward primer containing a Kpn-I site and reverse primer containing an 8XHis-tag and Xho-1 site. The amplicon was cloned into the Kpn-I and Xho-I sites of pcDNA6. Expression vector pcACE2.H345A-microbody that expressed the ACE2.H345A microbody was generated by overlap extension PCR using primers that overlapped the mutation. Full-length cDNA sequence, primer sequences and amino acid sequences are shown in Tables S1, S2, and S3.

Human Sera
Control and recovered patient sera were collected from patients through the NYU Vaccine Center with written consent under I.R.B. approval (IRB 20-00595 and IRB 18-02037) and were deidentified. Donor age and gender were not reported.

Cells
Vero E6, CaCO2, A549, ACE2.A549, BHK, Huh7 293T, Vero and CHME3 cells were cultured in Dulbecco's modified Eagle medium (DMEM) supplemented with 10% fetal bovine serum (FBS) and penicillin/streptomycin (P/S) at 37°C in 5% CO_2. CaCO2 cells were cultured in DMEM/10% FBS/1% nonessential amino acids. U937 cells were cultured in RPMI/10% FBS/ with P/S. ExpiCHO-S (Thermo Fisher Scientific) were cultured in ExpiCHO expression medium at 37 °C in 8% CO_2. Cell line ACE2 expression levels were quantified by staining with anti-ACE2 antibody (NOVUS) and Alexa Fluor 594-conjugated goat anti-mouse IgG (Biolegend) and pacific blue viability dye. Data were analyzed by flow cytometry with Flowjo software. ACE2.293T cells were established by lipofection of 293T cells with pLenti.ACE2-HA using lipofectamine 2000 (Invitrogen). After 2 days, the cells were selected in 1 μg/ml puromycin and cloned at limiting dilution. Single cell clones were expanded and analyzed by flow cytometry and a single clone was chosen. A549 cells were transfected with pLenti.ACE2 using lipofectamine 2000. After two days, the cells were selected in medium containing 1 μg/ml puromycin and cloned at limiting dilution. Individual cell clones were screened by flow cytometry for high ACE2 expression and a single cell clone was expanded.

METHOD DETAILS

SARS-CoV-2 Lentiviral Pseudotype Assay
SARS-CoV-2 spike protein pseudotyped lentiviral stocks were produced by cotransfecting 293T cells (4 X 10^6) with pMDL, pLenti.GFP-NLuc, pcCoV2.S and pRSV.Rev at a mass ratio of 4:3:4:1 by calcium phosphate coprecipitation. Additional spike protein

expression vectors were pcCoV2.S-Δ19, pcCoV2.S-Δ19.D614G or the β coronavirus RBD expression vectors. VSV-G pseudotyped lentivirus was similarly produced substituting the spike protein vector for pcVSV-G. Virus lacking an envelope glycoprotein was produced by using pcDNA6 in place of pcCoV2.S. Virus-containing supernatant was harvested 2 days post-transfection, passed through a 0.45 μm filter and concentrated by ultracentrifugation over a 20% sucrose cushion at 30,000 RPM for 90 minutes in an SW40.1 rotor in a Beckman Optima L-100K ultracentrifuge (Brea, CA). The pellet was resuspended to 1/10 the initial volume in DMEM/10% FBS and frozen in aliquots at −80°C. Virus stocks were titered on ACE2.293T by flow cytometry and reverse transcriptase activity using a real-time PCR assay (Vermeire et al., 2012).

To test for infectabilty of cell lines, the cells in a 96 well tissue culture dish at 1 X 10^4 cells/well were infected with pseudotyped lentivirus at MOI = 0.2. After 2 days, the culture medium was removed, 50 μls medium 50 and μls Nano-Glo luciferase substrate (Promega) was added and 70 μls was transferred to a microtiter plate which was read in an Envision 2103 microplate luminometer (PerkinElmer). To test the inhibitory activity of soluble receptors and convalescent sera, 50 μL serially diluted soluble receptor or serum was incubated for 30 minutes at room temperature with reporter virus (corresponiing to approximately 25 X 10^6 cps luciferase activity) at a MOI of 0.2 in a volume of 100 μl. The mixture was added to ACE2.293T cells in a 96 well tissue culture dish containing 1 X 10^4 cells/well and then cultured for 2 days. Luciferase activity was measured by Nano-Glo assay and GFP+ cells were quantified by flow cytometry with pacific blue viability dye (Biolegend). For antibody blocking, anti-ACE2 mAb (Novus) diluted 1:20 was added to the cells 30 minutes prior to infection.

Protein Purification and Molecular Mass Determination
293F cells (Thermo Fisher) at a density of 2.5 X 10^6 cells/ml were transfected with microbody expression vector plasmid DNA using polyethyleneimine (Polysciences, Inc) at a ratio of 1:3 plasmid:polyethyleneimine. The cells were then cultured at 30°C and at 12 hours post-transfection, 10 mM sodium butyrate was added. After 4 days, the culture medium was collected, filtered and adjusted pH to 8.0. The medium was passed over a 5 mL HiTrap Chelating column charged with nickel (GE healthcare), washed with 30 mL of buffer containing 20 mM Tris pH 8, 150 mM NaCl, 10 mM imidazole and the bound protein was eluted in buffer containing 250 mM imidazole. The eluate was concentrated to 1.0 mL and loaded onto a Superdex 200 size-exclusion column (GE healthcare) in running buffer containing 10 mM Tris pH 7.4, 150 mM NaCl. Protein containing fractions were pooled and concentrated. The purified proteins were analyzed on a 4%–12% Bis-Tris SDS-PAGE stained with Coomassie blue. The yield of pure protein was 4 mg/liter of culture.

The molecular masses of the purified protein complexes were determined by SEC/MALs. The proteins were injected onto a Superdex 200 10/300 GL gel-filtration chromatography column equilibrated in sample buffer connected to a Dawn Heleos II 18-angle light-scattering detector (Wyatt Technology), a dynamic light-scattering detector (DynaPro Nanostar; Wyatt Technology) and an Optilab t-rEX refractive index detector (Wyatt Technology). The data were collected at 25°C at a flow rate of 0.5 ml/minute every second. The molecular mass of each protein was determined by analysis with ASTRA 6 software.

Virion Pull-Down Assay
293T cells were transfected by lipofection with 4.0 μg pcACE2-microbody. At 72 hours post-transduction, 0.5 mL of culture supernatant was incubated with nickel-nitrilotriacetic acid-agarose beads (QIAGEN). The beads were washed, and bound protein was eluted with Laemmle loading buffer. The proteins were analyzed on an immunoblot probed with mouse anti-6X His antibody (Invitrogen) and horseradish peroxidase (HRP)-conjugated goat anti-mouse IgG secondary antibody (Sigma-Aldrich). The proteins were visualized and quantified using luminescent substrate on an iBright CL1000 (Invitrogen) gel imager. Ratios were calculated as spike protein divided by P24 band intensities on an identical exposure of the blot.

Immunoblot Analysis
Transfected cells were lysed in buffer containing 50 mM HEPES, 150 mM KCl, 2 mM EDTA, 0.5% NP-40, and protease inhibitor cocktail. Protein concentration in the lysates was measured by bicinchoninic protein assay and the lysates (40 μg) were separated by SDS-PAGE. The proteins were transferred to polyvinylidene difluoride membranes and probed with anti-HA mAb (Covance), mouse anti-His mAb (Invitrogen) and anti-GAPDH mAb (Life Technologies) followed by goat anti-mouse HRP-conjugated second antibody (Sigma). The blots were visualized using luminescent substrate (Millipore) on iBright CL1000.

Binding Assay
Soluble ACE2 proteins (10 μg) were mixed with 20 μL nickel beads for 1 hour at 4°C. Unbound protein was removed by washing the beads with PBS. The beads were resuspended in PBS and mixed with 40 μL pseudotyped lentiviral virions. After 1 hour incubation at 4°C, the beads were washed with PBS and resuspended in reducing Laemmli loading buffer and heated to 90°C. The eluted proteins were separated by SDS-PAGE and analyzed on an immunoblot probed with anti-p24 antibody (AG3.0) followed by goat anti-mouse HRP-conjugated second antibody.

Live SARS-CoV-2 Neutralization Assay
mNeonGreen SARS-CoV-2 (Xie et al., 2020) was obtained from the World Reference Center for Emerging Viruses and Arboviruses at the University of Texas Medical Branch. The virus was passaged once on Vero.E6 cells (ATCC CRL-1586), clarified by low-speed centrifugation, aliquoted, and stored at −80°C. The infectious virus titer was determined by plaque assay on Vero.E6 cells. Virus

neutralization was determined as previously described (Xie et al., 2020). ACE2.293T cells were seeded in a 96-well plate (1 X 10^4/well). The next day, mNeonGreen SARS-CoV-2 (MOI = 0.5) was mixed 1:1 with serially 2-fold diluted soluble ACE2 protein in DMEM/2% FBS and incubated for 1 hour at 37°C. The virus:protein mixture was then added to the ACE2 cells and incubated for 24 hours at 37°C in 5% CO_2. The cells were fixed with 4% paraformaldehyde, stained with DAPI and the green fluorescent cells were counted on a CellInsight CX5 Platform high content microscope (Thermo Fisher).

QUANTIFICATION AND STATISTICAL ANALYSIS

All experiments were performed in technical duplicates or triplicates and data were analyzed using GraphPad Prism (Version 7 7.0e). Statistical significance was determined by the two-tailed, unpaired t test. Significance was based on two-sided testing and attributed to $p < 0.05$. Confidence intervals are shown as the mean $\pm$ SD or SEM (*$p \leq 0.05$, **$p \leq 0.01$, ***$p \leq 0.001$, ****$p \leq 0.0001$).